uOttawa

Photogrammetric Bathymetry for the Canadian Arctic

Matus Hodul

Thesis submitted to the
Faculty of Graduate and Postdoctoral Studies
in partial fulfillment of the requirements
for the M.Sc. Degree in Physical Geography

Depatrment of Geography
Faculty of Arts
University of Ottawa

Supervisor:
Dr. Anders Knudby

Thesis Committee:
Dr. Luke Copland
Dr. Michael Sawada

Abstract

This study proposes and demonstrates a through-water photogrammetry approach for Satellite Derived Bathymetry (SDB), which may be used to map nearshore bathymetry in the Canadian Arctic. A four step process is used: First, a standard photogrammetric extraction is performed on 2 m resolution WorldView stereo imagery, then apparent depths are calculated by referencing submerged points to the extracted elevation of the water level seen in the image. Due to the effects of refraction, these apparent depths are underestimates, and a refraction correction factor is applied to convert to actual depths. Finally, tidal stage at the time of image acquisition is used to bring depths to chart datum. A post processing step may be applied to remove erroneous depths caused by water surface objects such as boats, debris, or large waves. This was demonstrated in six study areas across Nunavut, Canada to test its robustness under a variety of environmental conditions, including different seafloor types, and under varying sea states. The six study sites were (with vertical accuracy given in Root Mean Square Error/and vertical bias, both in meters): eastern Coral Harbour (1.18/0.03), western Coral Harbour (0.78/-0.32), Cambridge Bay (1.16/0.08), Queen Maud Gulf (0.97/0.13), Arviat (1.02/0.13), and Frobisher Bay, where bathymetry extraction largely failed due to unfavourable sea surface conditions. These findings show that the proposed method has similar or better vertical accuracy as currently established SDB approaches; however, it has several benefits over the established methods which make it better suited for the Arctic. Namely, not requiring the precise atmospheric correction necessary for physics-based models, which is difficult at high latitudes; as well as being able to function in heterogeneous seafloor environments and not needing *in-situ* calibration data like the empirical spectral ratio approach, better suiting it to remote Arctic waters which often lack existing bathymetric survey data.

Acknowledgements

First and foremost, I would like to thank Dr. Anders Knudby for giving me the opportunity to complete my Master's degree under his excellent guidance. Anders has always been extremely supportive of my academic efforts, and has been an invaluable help during my Master's program, as well as before, when I worked for him during my undergrad at Simon Fraser University. For that, I will be forever grateful.

I would also like to thank my thesis committee members Dr. Luke Copland and Dr. Michael Sawada for their advice and guidance in completing this project. I am grateful to Stephen Bird for providing his extensive technical expertise in photogrammetry. Thank you to my colleagues at the CHS Marc-André Faucher, Ryan Ahola, René Chénier, Loretta Abado, and many others, who helped make this thesis possible, and allowed me to use a great deal of CHS time, resources, and data on this project.

I would also like to thank the various organizations which funded this research and provided data and other resources. Support was provided by the Canadian Hydrographic Service, Canadian Space Agency, Government of Ontario, DigitalGlobe Foundation and Natural Sciences and Engineering Research Council.

I would like to extend my most sincere gratitude to my family and friends; I could not have finished this without their support. Thanks to Marie-Bé, Daniela, Connor, Loretta, Mary, and Jayne for helping me enjoy my time in Ottawa. Tusen takk to the fine folks at UNIS and all the people I met there, especially Ida, Arja, and Ju, for the best two months of my life. Finally, I would like to thank Mr. Bolognese for being the best high school geography teacher on the planet, and for inspiring me to study geography in university.

This thesis is dedicated to Branislav Hodúl.

Contents

List of Figures

List of Tables

Chapter 1

Introduction

Bathymetric data is vital to safe and effective marine transportation, resource exploitation, and recreation; especially in harbours, approaches, and other nearshore environments where shipping traffic is concentrated and the risk of grounding is high (IHO 2015). This data is communicated to mariners on nautical charts, along with shoreline position, the type and location of aids to navigation, and other such information necessary for safe navigation. In Canada, this is performed by the Canadian Hydrographic Service (CHS), which produces charts for all Canadian waters. However, surveys in much of the Arctic region remain limited, or were conducted using now outdated methods such as lead-line soundings (Chénier et al. 2016). As ice coverage in this region continues to decline, shipping traffic through these dangerous and remote waters will increase (OAG 2014), necessitating the creation of up-to-date navigational charts.

The primary method for obtaining modern bathymetric data is through ship-borne acoustic multibeam soundings, a method which delivers extremely accurate data, but is expensive and time consuming. In the Canadian arctic, such methods are being used to chart major shipping lanes and harbours (Chénier et al. 2017). However, smaller harbours and nearshore areas will likely never be surveyed to these standards due to the expense and time this would require.

Instead, the use of remote sensing techniques is being investigated by hydrographic offices and academic institutions, in order to provide relatively cheap and spatially extensive coverage, in a series of methods known collectively as Satellite Derived Bathymetry (SDB). Current SDB research and application focuses on three main types of method:

1. Empirical, colour based methods, which use *in-situ* depth survey data to create an empirical relationship between a spectral ratio, typically $blue/green$, and coincident depth (Stumpf et al. 2003).

2. Physics-based methods, which use a Radiative Transfer Model (RTM) to forward-model a range of seafloor spectral reflectances which would be expected given realistic combinations of environmental variables including seafloor type and depth. The model is then inverted by matching a pixel's radiance to the closest corresponding modelled value, and assigning it those variables (Knudby et al. 2016).

3. Wave Kinematics Bathymetry (WKB), which uses the linear dispersion equation to relate celerity of ocean swell waves to depth (Holland 2001), and has been implemented on spaceborne platforms using near-simultaneous image acquisition (Abileah 2006; de Michelle et al. 2012; Poupardin et al. 2014). This is the only SDB method which is able to map depth in highly turbid waters, as a view of the

seafloor is not necessary. However, it relies on optimal wave and sun angle conditions, making it impractical for broad global application.

The benefits and limitations of both empirical and physics-based approaches are detailed in Chapters 2 and 3. This thesis introduces an additional method: through-water satellite photogrammetry. Because photogrammetry relies on stereo geometry rather than spectral information, this method is able to perform better in certain conditions where the empirical or physics-based methods would be difficult or impossible to implement.

The SDB approach proposed by this thesis was innovated from field-based and airborne two-medium photogrammetry techniques. Though photogrammetry is a well-established tool for the extraction of *terrestrial* topography, bathymetric applications have been extremely limited. Most work in this direction has focused on producing extremely high-resolution maps of fluvial bathymetry from close-range photogrammetry or structure-from-motion, using ground-based methods (Butler et al. 2002; Bird et al. 2010), drones (Lejot et al. 2007; Woodget et al. 2015; Dietrich 2016), or aerial photography (Westaway et al. 2000; Westaway et al. 2003; Javernick et al. 2014). Murase et al. (2008) used aerial photogrammetry to successfully map ocean bathymetry. Expanding these methods to work with high-resolution satellites capable of stereo imagery is a natural development of this field, allowing for the photogrammetric method to be used in SDB applications for navigational charting.

1.1 Thesis Objectives

This thesis aims to develop an innovative method for Satellite Derived Bathymetry in Canada using the photogrammetric technique with the 2 m resolution WorldView-2 sensor, for the purposes of navigational charting. This objective is achieved by:

1. Demonstrating a proof-of-concept for the technique of Satellite Derived Bathymetry using through-water photogrammetry, which may be globally generalized using any high-resolution stereo-capable sensor and for any end-use scenario requiring bathymetry data in near-shore environments; and

2. Testing the method throughout the Canadaian Arctic, comparing its performance to that of currently established SDB methods, and investigating its usefulness in CHS charting operations.

To do this, this thesis presents two articles appropriate for publication in peer reviewed journals, corresponding to the two research objectives outline above:

1. ***Satellite Derived Photogrammetric Bathymetry***, in which the theoretical background for through-water photogrammetry is developed, and its effectiveness is demonstrated in Coral Harbour, Nunavut, an ideal study area. This paper is intended to stand on its own, with information which is broadly applicable to a global audience with any interest in near-shore bathymetric measurement.

2. ***Photogrammetric Bathymetry for the Canadian Arctic***, in which the technique developed in the first paper is applied in five ideal and non-ideal study areas throughout Nunavut. This paper is intended to supplement the first by applying the previously developed method in a variety of locations and under a variety of conditions to test its robustness and broad applicability.

This research was done in collaboration with the Remote Sensing department at the CHS (René Chénier) and Fluvial Systems Research Inc. (Stephen Bird), and contributes to a broader investigation into SDB

methodology being undertaken by the Shallow Water Earth Observation Lab (SWEOL) at University of Ottawa (Dr. Anders Knudby) and the CHS Remote Sensing Centre of Expertise (RSCoE).

1.2 Thesis Format

The two papers, *Satellite Derived Photogrammetric Bathymetry*, and *Photogrammetric Bathymetry for the Canadian Arctic* are presented here as Chapter 2 and Chapter 3 respectively. Figures and tables are presented in-text in appropriate location, and references cited in each chapter are given at the end of the corresponding chapter.

1.3 References

Abileah, R., 2006. Mapping shallow water depth from satellite. *ASPRS 2006 Annual Conference.*

Bird, S., Hogan, D., and Schwab, J., 2010. Photogrammetric monitoring of small streams under a riparian forest canopy. *Earth Surface Processes and Landforms, 35*, 952-970.

Butler, J.B., Lane, S.N., Chandler, J.H., and Porfiri, E., 2002. Through-water close range digital photogrammetry in flume and field environments. *Photogrammetric Record, 17(99)*, 419-439.

Chénier, R., Abado, L., Sabourin, O., and Tardiff, L., 2016. CHS Priority Planning Tool (CPPT): GIS approach for defining CHS surveying and charting priorities. *Canadian Hydrographic Conference, May 2016, Halifax, Nova Scotia.*

Chénier, R., Abado, L., Sabourin, O., and Tardiff, L., 2017. Northern marine transport corridors: Creation and analysis of northern marine traffic routes in Canadian Waters. *Transactions in GIS, 21*, 1085-1097.

de Michele, M., Leprince, S., Thibot, J., Raucoules, D., and Binet, R., 2012. Direct measurement of ocean waves velocity field from a single SPOT-5 dataset. *Remote Sensing of Environment, 199*, 266-271.

Dietrich, J.T., 2016. Bathymetric structure-from-motion: Extracting shallow stream bathymetry from multi-view stereo photogrammetry. *Earth Surface Processes and Landforms, 42*, 355-364.

Holland, T.K., 2001. Application of the linear dispersion relation with respect to depth inversion and remotely sensed imagery. *IEEE Transactions on Geoscience and Remote Sensing, 39(9)*, 2060-2072.

IHO, 2015. Manual on Hydrography. *International Hydrographic Organization.*

Javernick, L., Brasington, J., and Caruso, B., 2014. Modeling the topography of shallow braided rivers using structure-from-motion photogrammetry. *Geomorphology, 213*, 166-182.

Knudby, A., Ahmad, S.K., and Ilori, C., 2016. The potential for Landsat-based bathymetry in Canada. *Canadian Journal of Remote Sensing, 42(4)*, 367-378.

Lejot, J., Delacourt, C., Piégay, H., Fournier, T., Trémélo, M-L., and Allemand, P., 2007. Very high spatial resolution imagery for channel bathymetry and topography from an unmanned mapping controlled platform. *Earth Surface Processes and Landforms, 32*, 1705-1725.

Murase, T., Tanaka, M., Tani, T., Miyashita, Y., Ohkawa, N., Ishiguro, S., Suzuki, Y., Kayanne, H., and Yamano, H., 2008. A photogrammetric correction procedure for light refraction effects at a two-medium boundary. *Photogrammetric Engineering and Remote Sensing, 74(9)*, 1129-1136.

Office of the Auditor General of Canada, 2014. Marine Navigation in the Canadian Arctic. *In: Report of the Commissioner of the Environment and Sustainable Development.*

Poupardin, A., Michele, D.M., Raucoules, D., and Idier, D., 2014. Water depth inversion from satellite dataset. *IGARSS 2014.*

Stumpf, R.P., Holderied, K., and Sinclair, M., 2003. Determination of water depth with high-resolution satellite imagery over variable bottom types. *Limnology and Oceanography, 47(1)*, 547-556.

Westaway, R.M., Lane, S.N., and Hicks, D.M., 2000. The development of an automated correction procedure for digital photogrammetry for the study of wide, shallow, gravel-bed rivers. *Earth Surface Processes and Landforms, 25*, 209-226.

Westaway, R.M., Lane, S.N., and Hicks, D.M., 2003. Remote survey of large-scale braided, gravel-bed rivers using digital photogrammetry and image analysis. *International Journal of Remote Sensing, 24(4)*, 795-815.

Woodget, A.S., Carbonneau, P.E., Visser, F., and Maddock, I.P., 2015. Quantifying submerged fluvial topography using hyperspectral resolution UAS imagery and structure from motion photogrammetry. *Earth Surface Processes and Landforms, 40*, 47-64.

Chapter 2

Satellite Derived Photogrammetric Bathymetry

Matúš Hodúl [a,b], Stephen Bird [c], Anders Knudby [a], René Chénier [b]

[a] Department of Geography, Environment, and Geomatics. University of Ottawa, Ottawa,ON, Canada
[b] Canadian Hydrographic Service. Ottawa, ON, Canada
[c] Fluvial Systems Research Inc. White Rock, BC, Canada

Abstract

Satellite Derived Bathymetry (SDB) is being adopted as a cheaper and more spatially extensive method for bathymetric mapping than traditional acoustic surveys, with research being conducted by the Canadian Hydrographic Service under a Government Related Initiatives Program of the Canadian Space Agency. Established SDB methods involve either an empirical approach, where a regression between known depths and various colour indexes is developed; or a physics-based approach, where light interactions through the water column are simulated. Both methods have achieved vertical accuracies of around 1 m. However, the empirical approach is limited to areas with existing *in-situ* depth data, and is only applicable in homogenous benthic environments, while the physics-based approach requires precise atmospheric correction. This paper proposes a through-water photogrammetric approach which avoids these limitations by using feature extraction and image geometry rather than spectral radiance to estimate bathymetry. The method is demonstrated in Coral Harbour, Nunavut, Canada using a WorldView-2 stereo pair. A standard photogrammetric extraction was performed on the stereo pair, including a blunder removal and noise reduction. Apparent depths were then calculated by referencing under-water points to the extracted elevation of the water-line. Actual in-image depths were calculated from apparent depths by applying a correction factor to account for the effects of refraction at the air-water boundary. A tidal reduction brought depths to local chart datum, allowing for validation with Canadian Hydrographic Service survey data showing a mean vertical error of 0.031 m and an RMSE of 1.178 m. The method has a similar accuracy to the two established SDB methods, allowing for its use for bathymetric mapping in circumstances where the established methods are not applicable due to their inherent limitations.

2.1 Introduction

Bathymetric data of nearshore environments represents critical knowledge in fields such as maritime transport, coastal zone management, fisheries, environmental protection and management, marine science, maritime boundary delimitation, defence, tourism, and recreation (IHO 2005). Traditional bathymetric mapping is conducted using ship-borne acoustic surveys, which are extremely accurate but time-consuming, expensive, and not typically conducted in nearshore areas shallower than 4 m (Witmer et al. 2016). Satellite Derived Bathymetry (SDB) is being widely adopted as a relatively cheap and spatially extensive technique to support traditional surveys by filling gaps, monitoring changes in areas with highly dynamic seafloor features, and charting inadequately surveyed areas (Chenier et al. 2016). Under a Government Related Initiatives Program (GRIP) of the Canadian Space Agency (CSA), the Canadian Hydrographic Service (CHS) is investigating SDB as a method for chart updating. The current SDB methods in use can broadly be classified into two categories: a physics-based approach, which simulates light interacting with the water column and seafloor; and empirical models, which develop regressions between *in-situ* calibration data and spectral radiance.

The physics-based approach uses Radiative Transfer Models (RTM) to forward-model a range of possible sea-surface spectral radiances as a function of water quality, water depth, and bottom reflectance. This forward model is then inverted to estimate depth by identifying the modeled spectral radiance which most closely resembles that observed in each pixel (Lee et al. 1999; Hedley et al. 2009). Accuracies of up to 0.91 m Root Mean Square Error (RMSE), down to a depth of about 13 m, have been demonstrated under ideal conditions using airborne hyperspectral imagery (Dekker et al. 2011), though satellite-based applications have been less encouraging (Knudby et al. 2016a). The challenge of atmospheric correction over water (Nazeer et al. 2014), necessary to calculate the precise estimates of sea-surface reflectance needed for the modelling (Vahtmäe and Kutser 2007), remains a limiting factor, especially in Arctic regions with low sun elevations (Knudby et al. 2016b).

The empirical approach relies on *in-situ* bathymetric data to calculate a regression between a natural logarithmic band ratio, typically log(Blue)/log(Green), and the corresponding depth (Stumpf et al. 2003). In principle, this method is designed to work in heterogeneous benthic environments consisting of both light substrates (sand/rock) and dark substrates (vegetation), assuming no change in water quality across a scene. In practice however, performance in such environments is unsatisfactory (Su et al. 2014), requiring the omission of results over dark substrates, or the application of complicated, locally adapted models for each substrate (Vinayaraj et al. 2016). This method has been widely adopted by hydrographic offices for the purpose of navigational charting (Mavraeidopoulos et al. 2017), with accuracies similar to those found using a physics-based approach (Chenier et al. 2016).

This paper proposes a third option for SDB, which applies the photogrammetric technique in conjunction with a correction accounting for refraction at the air-water boundary. Because photogrammetry is a geometric operation which does not rely on accurate spectral information, no atmospheric correction is necessary, making it useful in areas where physics-based approaches perform poorly due to difficult atmospheric conditions such as low light, strong adjacency effect, high aerosol density, and variations in atmospheric state within a scene. It is also well suited for heterogeneous environments where the empirical approach is unreliable, and for areas lacking in-situ data where the empirical approach cannot be implemented. Such techniques have been used for close-range fluvial bathymetry using handheld (Bird et al. 2010) and Unmanned Aerial Vehicle (Dietrich 2017) platforms, as well as ocean bathymetry using airborne platforms (Murase et al. 2008), however this is the first study to demonstrate the method using satellite imagery, specifically WorldView-2.

Satellite photogrammetry relies on the known location and orientation of imaging sensors to triangulate point features in stereo imagery (Schenk 2005). A Rational Function Model (RFM) uses 80 Rational Polynomial Coefficients (RPCs) to convert between image-space (line and sample) and object-space (XYZ coordinates) in a block adjustment allowing for feature triangulation (Cheng 2011). The RPCs are defined based on ephemeris, the satellite's position in 3-dimensional space at the time of exposure, measured by GPS as in-track/cross-track positions/altitude; and attitude, the orientation of the sensor, measured by gyros and a star tracker as pitch/roll/yaw (Grodecki and Dial 2003) (Figure 2.1).

Positional bias may be introduced into a photogrammetrically extracted Digital Elevation Model (DEM) due to small errors in ephemeris and attitude measurements. These are, for the most part, translational, and spatially consistent throughout a scene (Fraser et al. 2006). Using only RPCs for image positioning, DigitalGlobe reports an accuracy of CE90 = 3.5 m (horizontal), and LE90 = 3.6 m (vertical) for WorldView-2 (DigitalGlobe 2016a). Correcting this bias involves constraining the RFM in a bundle block adjustment, using image tie points or external data such as Ground Control Points (GCPs). Tie points are created on land surface features which are identifiable in both images of a stereo pair, and help constrain the model by refining the relative position of the two images (Rupnik et al. 2016). Accuracy can be further improved with the introduction of GCPs; Hobie and Ginzler (2012) found that the use of 36 GCPs improved horizontal accuracy to 0.56 m and vertical accuracy to 0.32 m RMSE with WorldView-2.

This paper presents a proof of concept for the derivation of nearshore bathymetry from a photogrammetric extraction of stereo imagery. WorldView-2 imagery has been selected due to its extremely high 2 m spatial resolution and excellent positional accuracy, allowing for DEM extraction without the use of GCPs to attain a horizontal accuracy of 3-4 m. The principle can be easily extended to other high resolution, stereo-capable sensors, and can be implemented using any professional-level photogrammetry software suite.

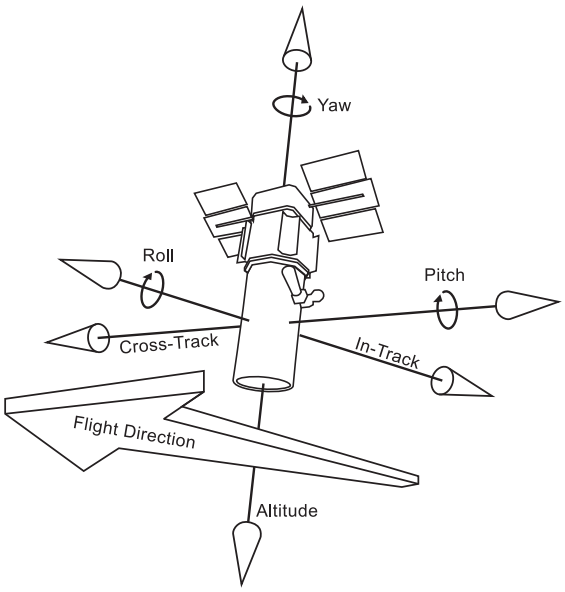

Figure 2.1: The six axes of movement, overlain over WorldView-2.

2.2 Study Area and Data

The Canadian Arctic provides an ideal location to develop the photogrammetric bathymetry approach, owing to its exceptionally clear water and a suitable benthic environment. Image matching algorithms used in photogrammetry software identify points or edges which are common to both images (Potuckova 2004), so it is necessary for the sea floor to contain relatively small, contrasting objects to provide adequate features for matching. Coral Harbour, in Nunavut, Canada (Figure 2.2), was selected as an ideal study area due to its large expanse of optically shallow water containing such features.

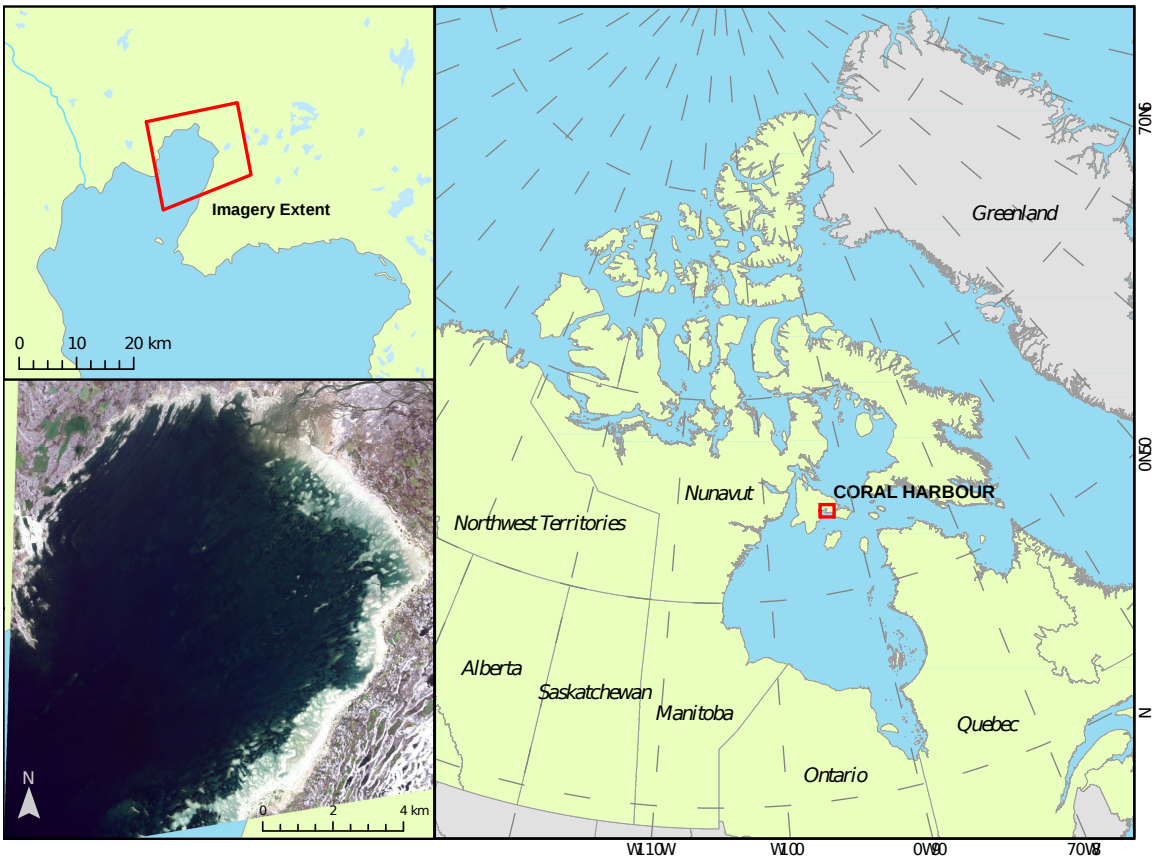

Figure 2.2: Location of the study area, Coral Harbour. Satellite image courtesy of the DigitalGlobe Foundation.

Considerations for imagery selection included the time of year, as the area is only clear of sea ice in late summer; lack of waves or ripples, which would affect stereo feature matching and refraction correction; and water clarity for a maximized optical extinction depth, as occasionally the area is inundated with suspended sediment. A summary of the selected stereo pair is shown in Table 2.1.

Table 2.1: Information on the WorldView-2 stereo pair used in this study. Dates in yyyy-mm-dd and times in UTC. Approximate scene center is 64.13°N, 83.05°W.

Digital Globe Catalog ID	10300100065FFF00	1030010006679B00
Acquisition Date & Time	2010 - 07 - 06 - 17:25:09	2010 - 07 - 06 - 17:26:39
Mean Off-Nadir View Angle	7.9°	32.0°
Mean Cross-Track View Angle	-2.4°	-3.5°
Mean In-Track View Angle	7.5°	-31.8°

Multispectral imagery in *Stereo Ortho-Ready 2A* format, with a spatial resolution of 2 m, was used in all processing steps. Though terrestrial photogrammetric work benefits from the improved 0.5 m spatial resolution of the panchromatic band or a pansharpened dataset, the unique requirements of through-water photogrammetry make this approach problematic. The spectral response of the panchromatic band in WorldView-2 data skews heavily towards the red and near-infrared (NIR) wavelengths (Figure 2.3), severely limiting its water-penetrating ability. Pansharpening the multispectral data has a similar detrimental effect.

Validation data was provided by the Canadian Hydrographic Service as 10,978 point depth measurements, of which 892 overlapped with the extracted bathymetry, with a vertical datum represented as *Chart Datum*, defined as the mean lower low water at large tide for Coral Harbour (DFO 2016).

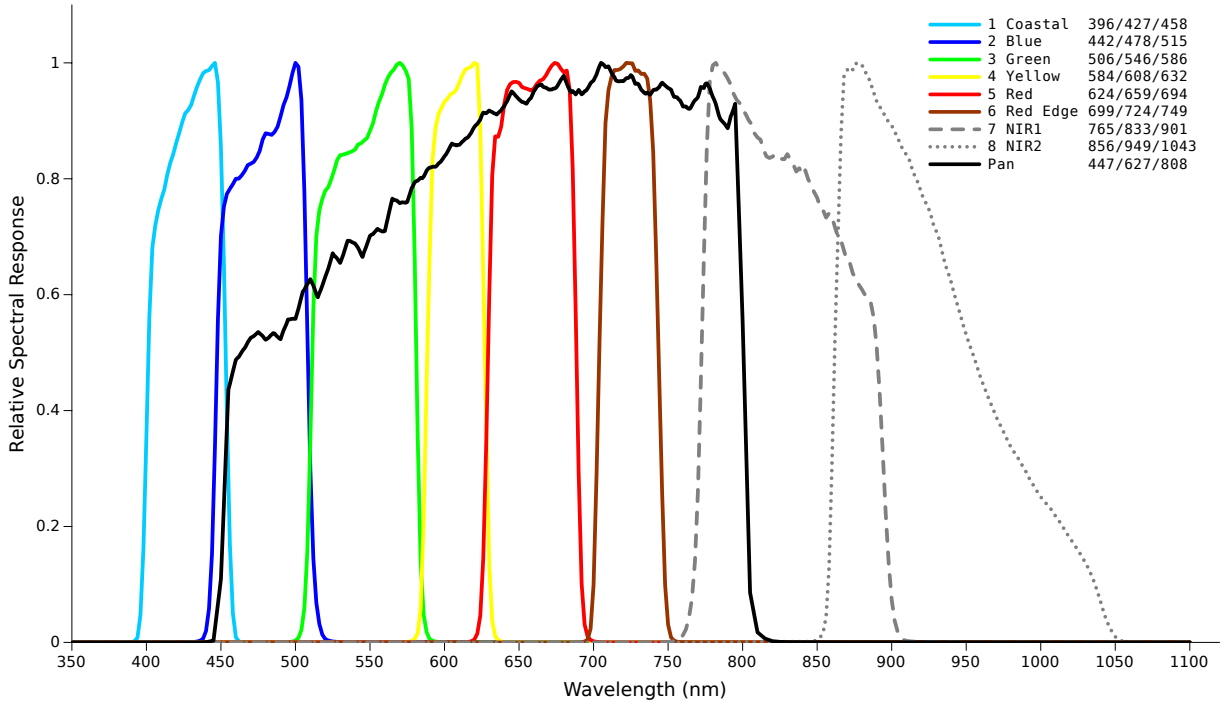

Figure 2.3: Radiometric response curves for WorldView-2 (Digital Globe 2016b). Values in legend indicate lower band edge/central wavelength/upper band edge, all in nm (Digital Globe 2016c). The panchromatic band skews heavily towards red and near-infrared bands wavelengths, making its water-penetrating ability very limited.

2.3 Methods

The method consisted of four main processing steps: photogrammetric extraction, error and noise removal, refraction correction, and datum reduction.

2.3.1 Photogrammetric Extraction

PCI Geomatica was used for the photogrammetric extraction. A standard bundle block adjustment was performed on the stereo pair using the RPCs provided with the imagery, and land-based tie points. These were generated automatically through image correlation for every individual spectral band, then added to the bundle block. A manual check was performed to remove tie points generated on the water surface, moving objects, and mismatches on objects with a repeating pattern.

The Green band (Band 3) was used for the photogrammetric extraction because it was visually determined that seafloor features at a broad range of depths were most visible at this wavelength (Figure 2.4). This will likely vary depending on site-specific bottom types and water quality and should be determined individually for application in other sites.

Photogrammetric extraction proceeded by generating epipolar image pairs, in which the stereo pairs were re-oriented such that parallax lay on a common axis. Image correlation then proceeded in one-dimensional space, reducing processing time and improving accuracy. Matched features were triangulated with the exposure station locations and orientations, resulting in ground surface points in three dimensions relative to the ellipsoid. Points were then averaged into a DEM with a 5 m horizontal resolution.

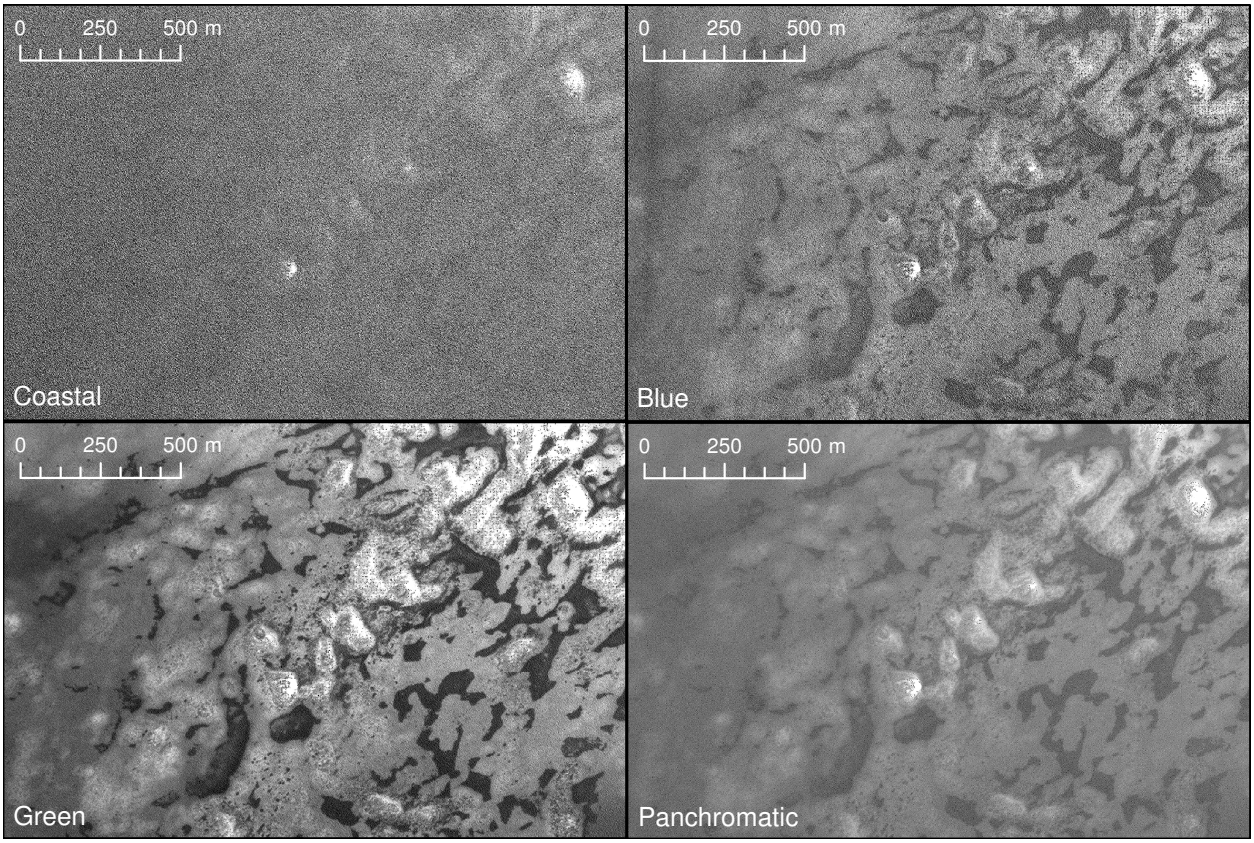

Figure 2.4: A subset of the Coral Harbour imagery, showing a comparison between the four WorldView-2 bands useful for through-water analysis: Band 1 - Coastal; Band 2 - Blue; Band 3 - Green; and the panchromatic band. Seafloor features are most visible and sharply resolved in the green band, which was thus used for the photogrammetric extractions.

2.3.2 Error Identification and Removal

Filtering of the generated point cloud must account for two main error types: low magnitude, high frequency errors— noise; and high magnitude, low frequency errors— blunders (Milledge et al. 2009). The filtering process must use a multi-level system to account for the two types of point error. Specifically, it is necessary to first remove or replace blunder points in order to prevent these errors propagating to neighbouring points during a smoothing procedure.

During DEM extraction, Geomatica outputs a correlation score for each pixel of the DEM on a 0-100 scale. To remove blunders, a threshold may be set such that pixels below a certain score will be removed

from the DEM. A threshold of 70 was chosen here, determined to be an adequate balance between removing blunders and retaining useful data. A 5x5 pixel mean filter was subsequently applied to reduce noise caused by the photogrammetric extraction process.

2.3.3 Refraction Correction

Due to the effects of optical refraction at the air-water boundary, feature depths are underestimated by the stereo extraction (Figure 2.5), requiring a refraction correction.

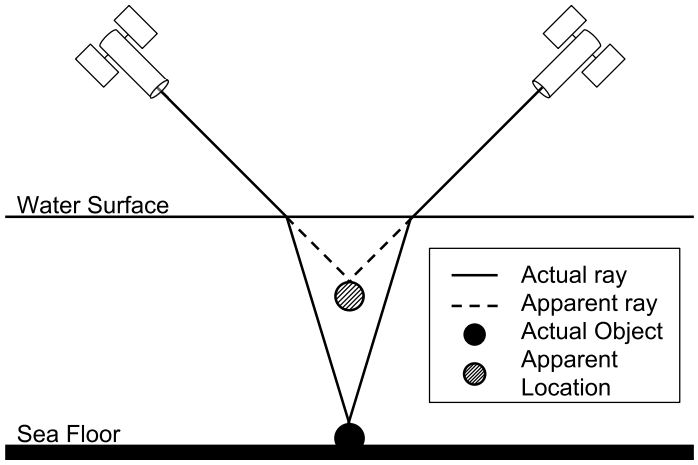

Figure 2.5: Simplified diagram illustrating the effect of refraction on the triangulation of point features in through-water photogrammetry, where features appear shallower than they actually are.

Stereo output data shows topographical elevations relative to the ellipsoid, however the refraction correction must be applied to apparent water depths at the time of imagery acquisition. To do this, the water surface elevation relative to the ellipsoid was determined using an orthorectified version of one of the images in the stereo pair. The near-infrared Band 8 was thresholded to create a water mask, which was then converted into a polygon representing water surface along whose edge several thousand points were generated. Some manual editing was done to remove erroneous points which obviously were not located on the waterline. Elevation values at the remaining points representing the height of the waterline relative to the ellipsoid were extracted, the mode of these values was taken as the height of the water surface, and was subtracted from below-water topography values giving *apparent* water depth.

Actual water depth was then calculated from the apparent water depth using a refraction correction procedure. Murase et al. (2008) developed a comprehensive two-media refraction correction method for aerial photography, which was adapted here.

Due to the curvature of the Earth, imagery incidence angles in off-nadir imagery are slightly larger than the view angles shown in Table 2.1 (Figure 2.6). These can be calculated from view angles using Equation 2.1, where α is the view angle, β is the incidence angle, H if the orbital altitude of the sensor, and R is the radius of the Earth. Radius R varies slightly with latitude φ, and may be calculated using Equation 2.2, where R_e and R_p are the radius at the equator (6378.137 km) and pole (6356.752 km) respectively. WorldView-2 orbital altitude is approximately 770 km.

$$\beta = \sin^{-1}\left(\frac{R+H}{R}\sin\alpha\right) \tag{2.1}$$

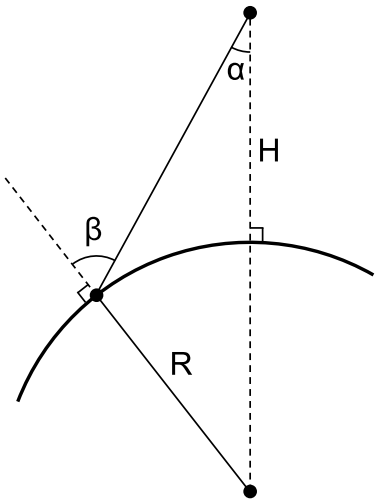

Figure 2.6: Illustration of the difference in view angle α and incidence angle β. H and R are sensor orbital altitude and Earth radius respectively. Scale has been exaggerated to demonstrate the effect; in reality, α and β differ by only a few degrees for typical scene geometries of WorldView-2 stereo imagery.

$$R(\varphi) = \sqrt{\frac{(R_e^2 \cos\varphi)^2 + (R_p^2 \cos\varphi)^2}{(R_e \cos\varphi)^2 + (R_p \cos\varphi)^2}} \tag{2.2}$$

Actual water depth h can then be related to the apparent water depth h_a as:

$$h = \frac{\tan r_A \cos\theta_A + \tan r_B \cos\theta_B}{\tan i_A \cos\theta_A + \tan i_B \cos\theta_B} * h_A \tag{2.3}$$

where r_A and r_B are incidence angles, calculated from off-nadir angles of each exposure A and B, θ_A and θ_B are the view azimuth angles (Figure 2.7),

$$i_A = \sin^{-1}\left(\frac{\sin r_A}{n}\right) \tag{2.4}$$

$$i_B = \sin^{-1}\left(\frac{\sin r_B}{n}\right) \tag{2.5}$$

and n is the refractive index of water, for which a value of 1.34 is accurate over a wide range of temperatures and salinities (Jerlov 1976). Because of the relatively small field of view of WorldView-2 and similar high-resolution satellites, image geometry does not vary by more than about 1° across a swath, meaning that the application of a single correction factor for the entire scene is an acceptable approximation (see Discussion). θ can be calculated for each exposure as:

$$\theta = \tan^{-1}\left(\frac{\tan\delta_c}{\tan\delta_i}\right) \tag{2.6}$$

where δ_c and δ_i are the cross-track and in-track components of the incidence angle respectively, calculated from cross-track and in-track view angles (Table 2.1) using Equation 2.1.

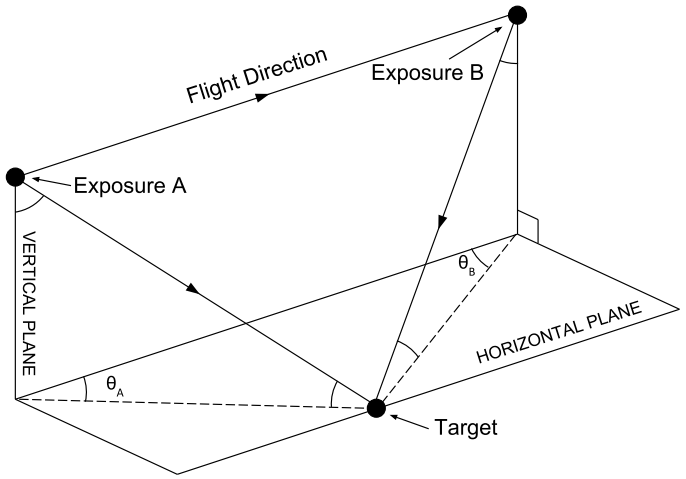

Figure 2.7: Three-dimensional geometry of a stereo pair relative to image center. θ_A and θ_B are the horizontal azimuth angles relative to flight direction.

2.3.4 Datum Reduction

After the application of the refraction correction, the bathymetric data represents water depths at the time of image acquisition. Depending on the intended use of the data, it may be desirable to perform a datum reduction to convert these to more useful values. In this paper, depths are reduced to the *chart datum* in Coral Harbour to correspond with validation data. Tidal stage relative to chart datum at image acquisition was modelled using the Toulouse Unstructured Grid Ocean Model (Pairaud et al. 2008; Collins et al. 2011), for station *06240 Coral Harbour NU*, and subtracted from in-image depths. Chart datum represents the lowest possible tidal level in the area, so negative depths are a common occurrence in bathymetric data of the nearshore, representing areas which are *usually* submerged, but dry when the tide level is at chart datum.

2.4 Results

The bundle block adjustment, using a total of 587 land-based tie points, resulted in a residual of 0.067 pixels, or 0.134 m. The ellipsoidal DEM heights of generated waterline points are shown as a histogram in Figure 2.8. A mode of -43.02 m was subtracted from the DEM to convert to apparent depths.

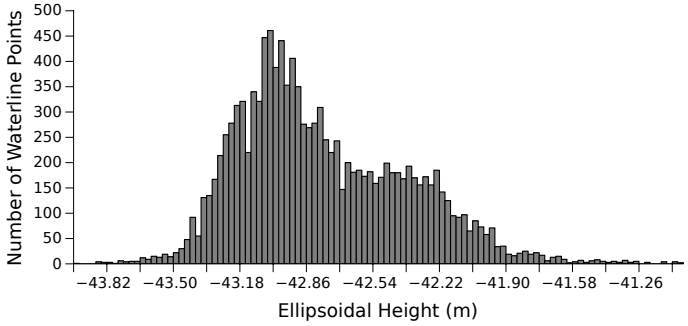

Figure 2.8: Histogram of ellipsoidal heights for generated water-line points. A mode of -43.02 m was used to convert ellipsoid heights to apparent depths.

Figure 2.9 shows scatterplots of photogrammetric depths after blunder and noise removal, against validation data, following each processing step:

A **Apparent depths**, after waterline correction using the -43.02 m waterline height. A regression line is fit to the data showing the underestimation of depths caused by refraction.

B **Actual depths** at the time of image acquisition. Using Equations 2.1 through 2.6, the refraction correction factor was calculated as 1.467, and applied to apparent depths to give actual depths.

C **Depths relative to chart datum.** A tidal stage of 1.105 m ±0.096 m was modeled, and subtracted from the actual depths, bringing the photogrammetric bathymetry into the same vertical datum as the validation data. Mean error may be used as a measure of the success of the tidal reduction process, including the waterline height extraction method, as it can reveal systematic bias in photogrammetric data (Lane et al. 2000). Here, a mean error of 0.031 m shows the method had worked well, to within the 10 cm error of the tidal prediction.

After these three processing steps, comparison with the validation data shows an RMSE of 1.178 m, which is similar to accuracies reported with empirical and physics-based approaches.

The derived bathymetry for the full scene is shown in Figure 2.10. For clarity, "depths" resulting from water surface objects have not been removed, however this may easily be done with a visual inspection and manual DEM editing typical of photogrammetric post-processing. The method was able to estimate bathymetry along the entire coast of the bay, as well as indicate the position and depth of shoals in the centre of the bay. As depths increased, feature matching became more difficult and fewer accurately matched points at large depths led to gaps in the bathymetry once the correlation factor threshold was applied. A depth of approximately 10 m was the effective limit. However Figure 2.9 shows that for points that were correlated at these depths, there appears to be no significant reduction in accuracy. Figure 2.10A shows the spatial distribution of residuals across the study area, which appear to have no broad pattern. The majority of large residuals occur over areas which contain obvious errors in bathymetry which could be removed in a post-processing step.

Figure 2.11 shows details of the estimated bathymetry, from sections outlined by black boxes in Figure 2.10. The panels A and B, showing true colour and overlain bathymetry respectively, demonstrate

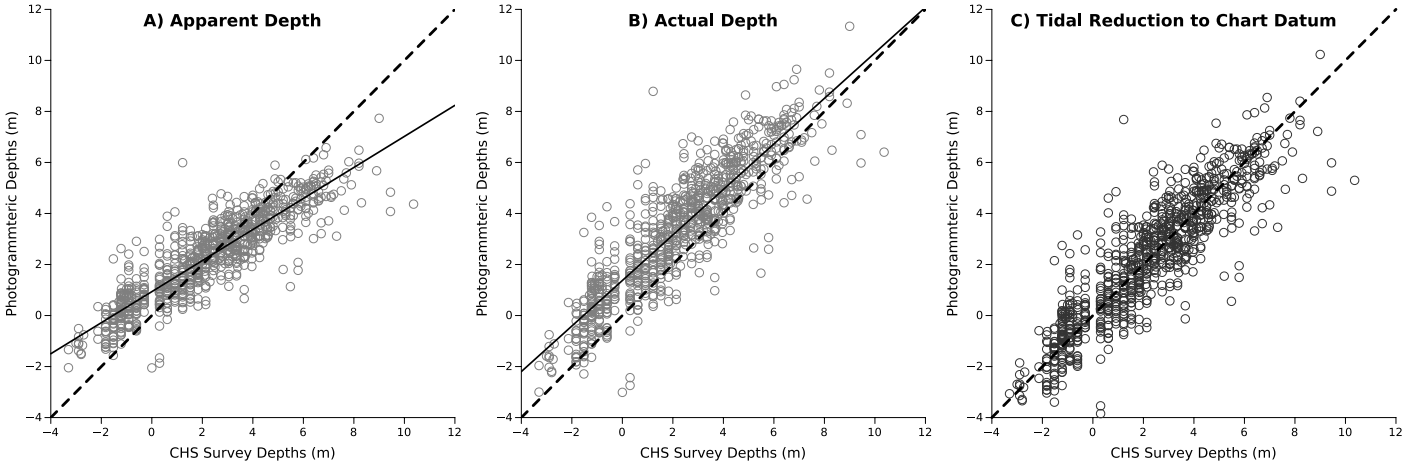

Figure 2.9: Scatterplot of photogrammetric bathymetry against survey depths: A) after waterline correction, B) after refraction correction, and C) after tidal reduction. Dashed line indicates x=y, solid line indicates linear regression.

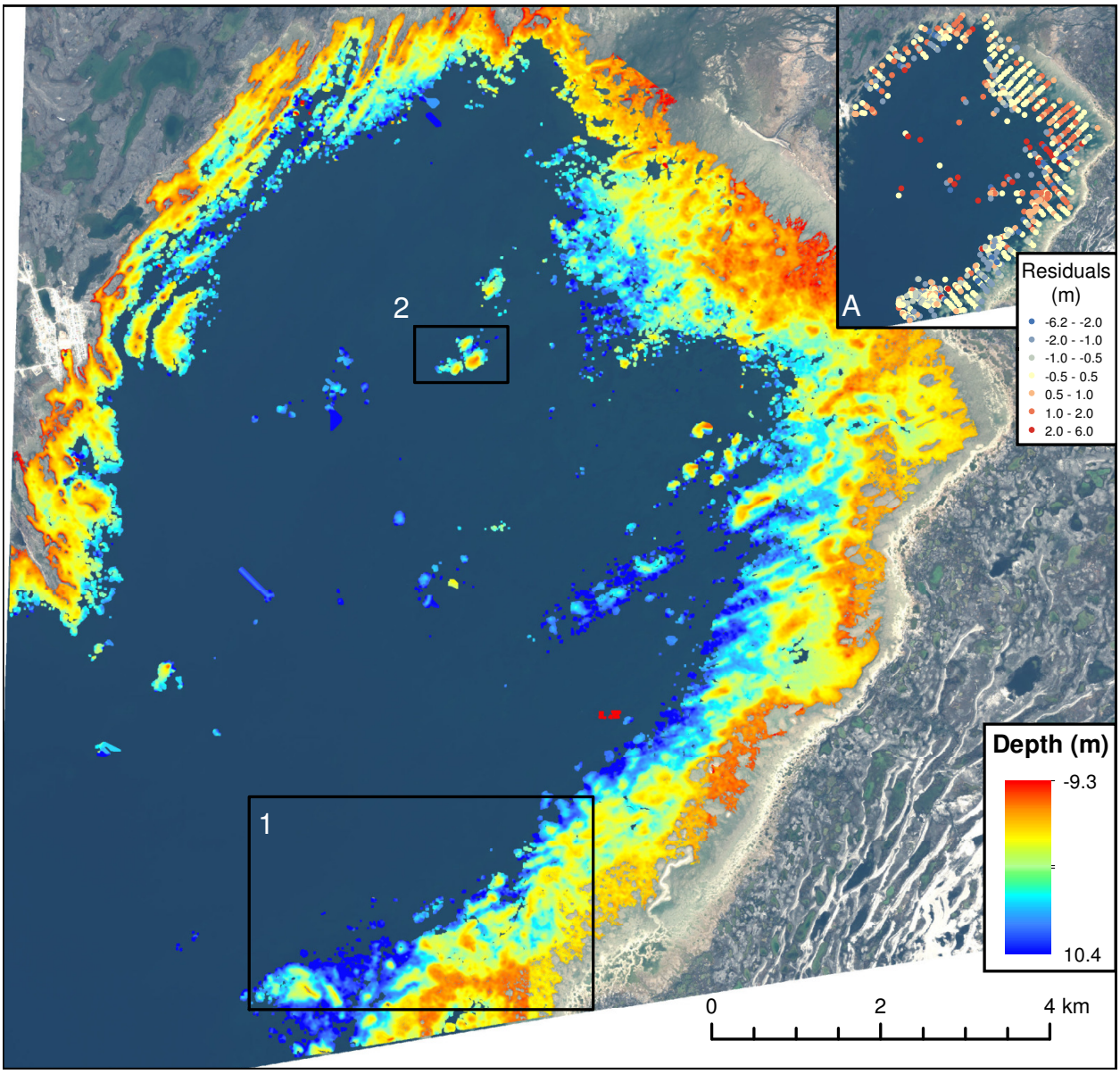

Figure 2.10: Photogrammetrically derived bathymetry, with depths relative to chart datum, for the complete Coral Harbour scene. Black boxes indicate the selections shown in Figure 2.11, with box 1 corresponding to panels A and B in Figure 2.11, and box 2 corresponding to C and D. Inset A shows the spatial distribution of residuals. Satellite image courtesy of the DigitalGlobe Foundation.

the need for contrasting features in the benthic environment. Small gaps in bathymetry data are present throughout, caused because the center of featureless dark patches were unable to be correlated. Additionally, the depth-dependent correlation effect is seen here: at small depths (< 3 m), almost the entire surface is correlated and bathymetry generated, while at depths past about 8 m, correlation and bathymetry data is sparse. The panels C and D show a case where the position and depth of a shoal have been identified, a case of particular interest to hydrographers.

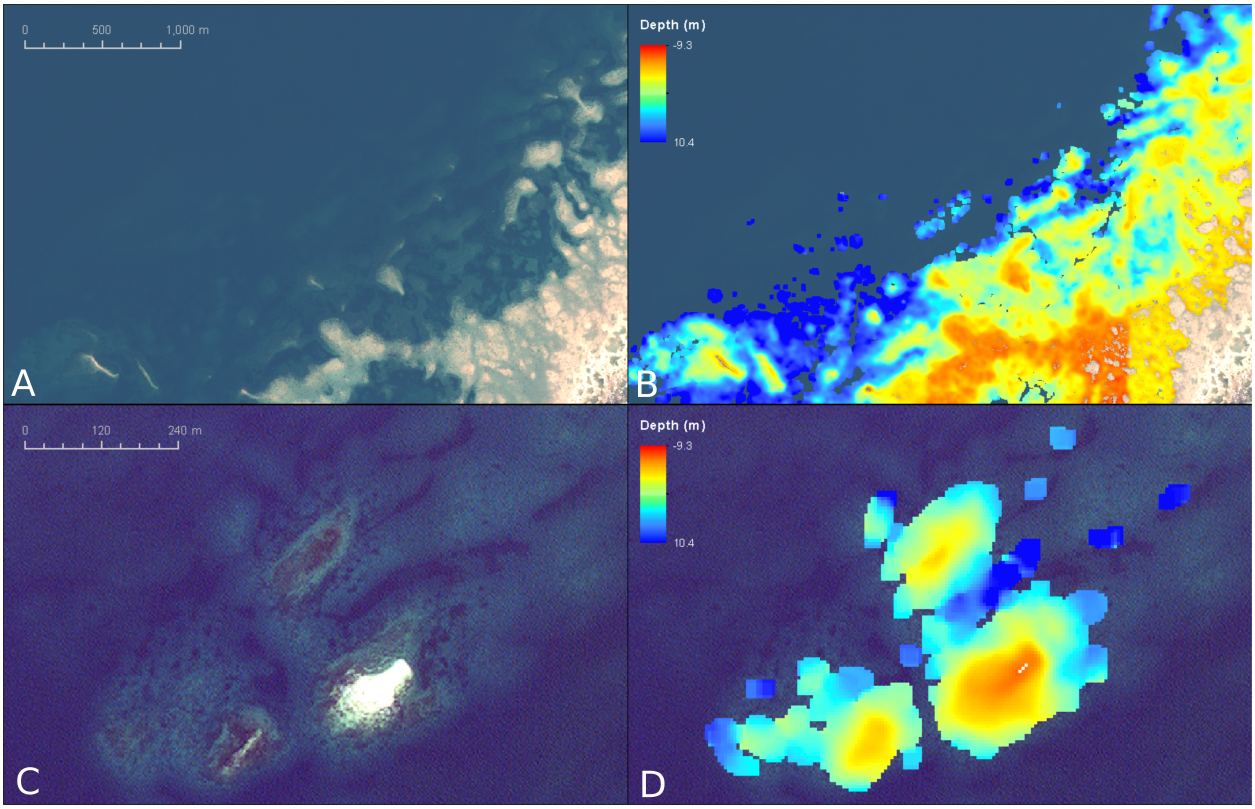

Figure 2.11: Details of the estimated bathymetry with depths relative to chart datum, from sections outlined by black boxes in Figure 2.10.

2.5 Discussion

Photogrammetric bathymetry provides a promising new option for bathymetric mapping, similar in accuracy to the empirical and physics-based SDB methods, and applicable in circumstances where the established methods perform poorly or are not possible to implement due to environmental conditions or lack of calibration data. Additionally, the method is extremely fast to implement, taking only a few hours for an entire WorldView-2 scene including all pre- and post-processing steps. The only important environmental limiting factor, other than the typical SDB need for clear water, is the necessity for small contrasting benthic objects needed for feature matching. As a result, the method may be limited in environments with large expanses of featureless seafloor such as sand or mud.

The refraction correction method makes the assumption that the angular geometry of the images, depicted in Figure 2.7, remains constant for every pixel within each image, allowing for a single correction factor to be applied to the entire DEM. In reality, r and θ vary slightly due to the cross-track field of view and in-track movement characteristic of pushbroom sensors. Image Support Data (ISD) gives minimum, maximum, and mean angles for these, which for the Coral Harbour imagery are shown in Table 2.2. The correction factor used in this study was calculated using the mean values, representing image centre; calculating correction factors using minimum and maximum values gives the range across the DEM. For the Coral Harbour imagery, these correction factors range between 1.462 and 1.471, which lead to a *maximum* possible variation in elevation at the scene edges of about 1 cm per metre of depth. Scenes with larger swath lengths will have higher variances due to geometry, so it may be desirable to apply a spatially varying correction factor for these.

Table 2.2: Angular geometry of the Coral Harbour stereo pair. All values in degrees.

Image	10300100065FFF00	1030010006679B00
Min Cross-Track View Angle	-2.6	-3.7
Max Cross-Track View Angle	-2.2	-3.3
Mean Cross-Track View Angle	-2.4	-3.5
Min In-Track View Angle	7.4	-32.3
Max In-Track View Angle	7.6	-31.3
Mean In-Track View Angle	7.5	-31.8
Min Off-Nadir View Angle	7.8	31.5
Max Off-Nadir View Angle	8.1	32.5
Mean Off-Nadir View Angle	7.9	32.0

Additionally, it must be assumed that the refractive boundary is planar (Rinner 1969), which in this case would refer to an absence of waves larger than about a pixel, otherwise r would vary greatly throughout a scene with wave shape. However, Fryer and Kniest (1985) found that in imagery acquired from high flying altitudes (i.e. small scales), random observation errors become much larger than error from waves. Since it is impossible at present to precisely model refraction through individual waves in satellite imagery, it remains advisable to carefully select for imagery with calm water.

Robust blunder detection remains an issue for further research. Thresholding of the correlation score for each point is an effective way to remove obvious errors in feature matching and improve the confidence in depth estimation of the remaining points. Figure 2.12 shows validation scatter plots containing the DEM without blunder removal, with highlighted points belonging to each of the indicated correlation score intervals. The 70-100 interval retained for the results shows no major blunders. The 60-69 interval shows many good points, but also several major blunders, and the 50-59 and 40-49 intervals have an even greater proportion of blunder points. A depth-dependence of correlation score is also evident, with poorer correlation as depth increases, which is why far fewer points remain in the bathymetry at greater depths than shallower depths.

Water surface objects such as boats, ice, buoys, and animals may have a high correlation score because their shape is coherent between the two images. Time between exposures in WorldView-2 stereo data is typically slightly longer than a minute (in this imagery, 1 minute and 29 seconds), allowing these objects to move perceptibly between exposures. If these objects move in the same direction as topographical parallax, they will be triangulated as having incorrect elevation, depending on the distance and direction of movement. Large errors are easily identified as having unfeasible "elevation", but smaller errors resulting in a similar "elevation" as the surrounding bathymetry are more difficult to detect. Currently, these effects may be fixed by visually identifying and removing the erroneous points, which is standard for photogrammetric post-processing, though for large scenes somewhat impractical.

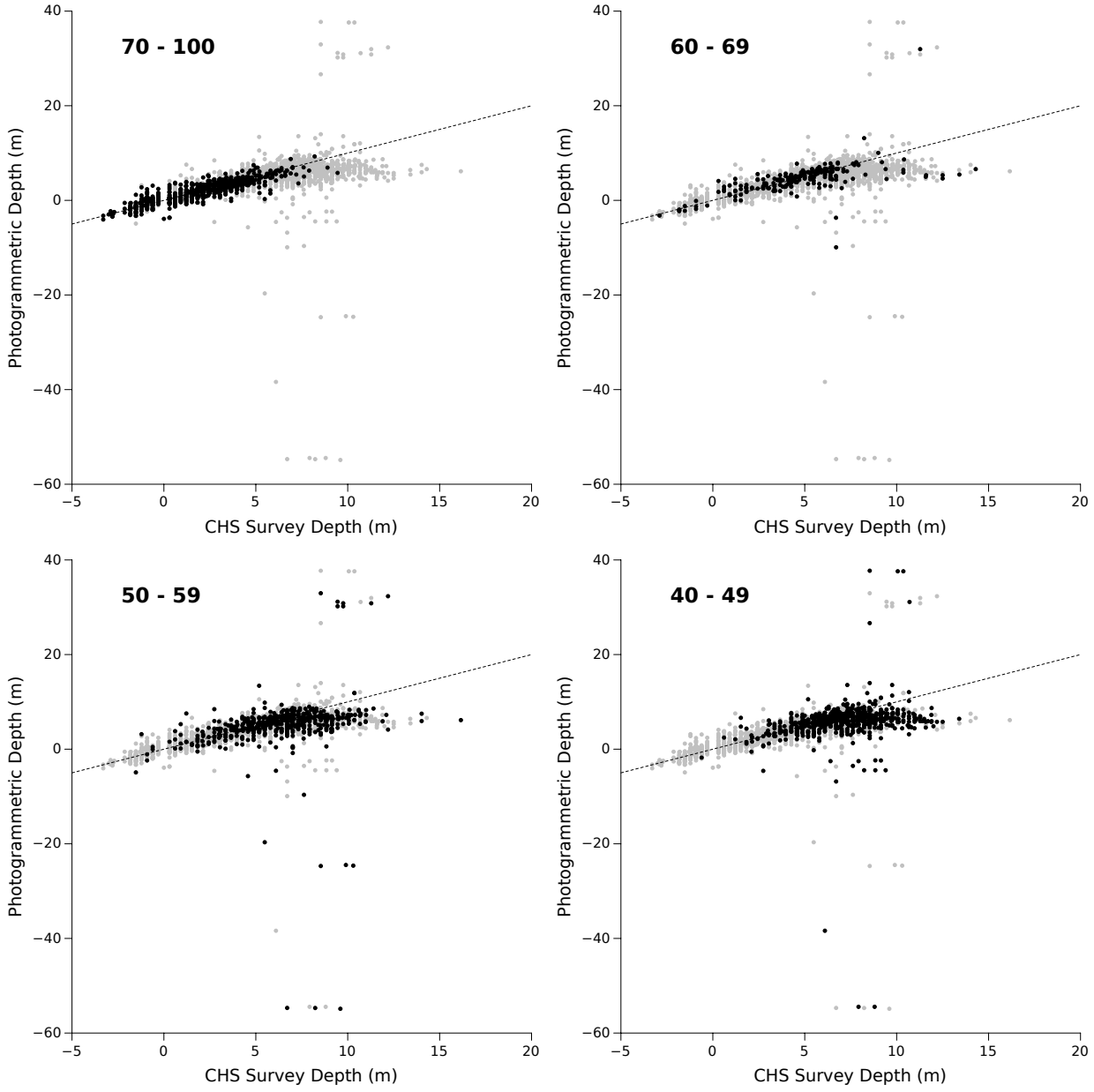

Figure 2.12: Scatterplots of the complete bathymetry against survey data. The complete dataset is shown as grey, while the indicated correlation score interval points are highlighted as black. Dashed line indicates x=y.

2.6 Conclusion

This paper has demonstrated that WorldView-2 stereo imagery can be used to extract bathymetric data to an accuracy similar to that of established SDB methods. A standard stereo extraction is performed on the data, including blunder removal and smoothing, after which a refraction correction is applied based on off-nadir positions of the sensor at each exposure, and a tidal reduction is done to translate at-image depths to a desired vertical datum. Coral Harbour, Nunavut, Canada was used to test this approach, showing an accuracy of RMSE = 1.178 m to a depth of 10 m. Photogrammetric Bathymetry has advantages over established methods because it does not rely on precise radiometry, so can be used in environments in which those methods would be restricted. The principle shown here can be easily extended to other high resolution, stereo-capable sensors, and can be implemented using any professional-level photogrammetry software suite.

2.7 Acknowledgments

The authors would like to acknowledge the Government of Ontario, the National Science and Engineering Research Council, the Canadian Hydrographic Service, and the Government Related Initiatives Program of the Canadian Space Agency for funding; Ryan Ahola, Marc-André Faucher, and Loretta Abado for help and advice, Lucas Green for drawing Figure 2.1, and DigitalGlobe Foundation for providing the imagery.

2.8 References

Bird, S., Hogan, D., and Schwab, J., Photogrammetric monitoring of small streams under a riparian forest canopy. *Earth Surface Processes and Landforms, 35*, 952-970.

Cheng, P., 2011. Geometric correction and automated DEM extraction of WorldView stereo data. *32nd Asian Conference on Remote Sensing, ACRS 2011.1.* 426-431.

Chenier, R., Faucher, M.A., Ahola, R., Jiao, X., and Tardif, L., 2016. Remote sensing approach for updating CHS charts. *Canadian Hydrographic Conference, May 16-19, Halifax.*

Collins, A.K., Hannah, C.G., and Greenberg, D., 2011. Validation of a high resolution modelling system for tides in the canadian arctic archipelago. *Canadian Technical Report of Hydrography and Ocean Sciences*, 273.

Dekker, A.G., Phinn, S.R., Anstee, J., Bissett, P., Brando, V.E., Casey, B., Fearns, P., Hedley, J., Klonowski, W., Lee, Z.P., Lynch, M., Lyons, M., Mobley, C., and Roelfsema, C., 2011. Intercomparison of shallow water bathymetry, hydro-optics, and benthos mapping techniques in Australian and Caribbean coastal environments. *Limnology and Oceanography: Methods, 9*, 396-425.

Department of Fisheries and Oceans, 2016. Chart No. 1: Symbols, abbreviations, and terms. *Canadian Hydrographic Service, Government of Canada.*

Dietrich, J.T., 2017. Bathymetric structure-from-motion: Extracting shallow stream bathymetry from multi-view stereo photogrammetry. *Earth Surface Processes and Landforms, 42*, 355-364.

Digital Globe, 2016a. Accuracy of Worldview Products. *From DigitalGlobe White Papers:* www.digitalglobe.com/resources/white-papers

Digital Globe, 2016b. WorldView-2 relative radiometric response curves. *From DigitalGlobe Technical Information:* www.digitalglobe.com/resources/technical-information

Digital Globe, 2016c. Spectral response for DigitalGlobe earth imaging instruments. *From DigitalGlobe Technical Information:* www.digitalglobe.com/resources/technical-information

Fraser, C.S., Dial, G., and Grodecki, J., Sensor orientation via RPCs. *ISPRS Journal of Photogrammetry and Remote Sensing, 60(3)*, 182-194.

Fryer, J.G., and Kniest, H.T., 1985. Errors in depth determination caused by waves in through-water photogrammetry. *Photogrammetric Record, 11(66)*, 745-753.

Grodecki, J., and Dial, G., 2003. Block adjustment of high-resolution satellite images described by rational polynomials. *ASPRS Journal of Photogrammetry and Remote Sensing, 1(10)*, 59-68.

Hedley, J., Roelfsema, C., and Phinn, S.R., 2009. Efficient radiative transfer model inversion for remote sensing applications. *Remote Sensing of Environment, 113(11)*, 2527-2532.

Hobi, M.L., and Ginzler, C., 2012. Accuracy assessment of digital surface models based on WorldView-2 and ADS80 stereo remote sensing data. *Sensors, 12*, 6347-6368.

IHO 2005. Manual on Hydrography.

Knudby, A., Ahmad, S.K., and Ilori, C., 2016a. The potential for Landsat-based bathymetry in Canada. *Canadian Journal of Remote Sensing, 42(4)*, 367-378.

Knudby, A., Roy, D., Ahmad, S.K., Bird, S., and Ilori, C. 2016b. Satellite-derived bathymetry for Canada. *Canadian Hydrographic Conference, May 16-19, Halifax.*

Jerlov, N.G., 1976. Marine optics. Elsevier Science and Technology.

Lane, S.N., James, T.D., and Crowell, M.D., 2000. Application of digital photogrammetry to complex topography for geomorphological research. *Photogrammetric Record, 16*, 793-821.

Lee, Z.P., Carder, K.L., Mobley, C.D., Steward, R.G., and Patch, J.F., 1999. Hyperspectral remote sensing for shallow waters 2: Deriving bottom depths and water properties by optimization. *Applied Optics, 38(18)*, 3831-3843.

Mavraeidopoulos, A.K., Pallikaris, A., and Oikonomou, E., 2017. Satellite derived bathymetry (SDB) and safety of navigation. *The International Hydrographic Review, 17*, 7-19.

Milledge, D.G., Lane, S.N., and Warburton, J., 2009. The potential of digital filtering of generic topographic data for geomorphological research. *Earth Surface Processes and Landforms, 34*, 63-74.

Murase, T., Tanaka, M., Tani, T., Miyashita, Y., Ohkawa, N., Ishiguro, S., Suzuki, Y., Kayanne, H., and Yamano, H., 2008. A photogrammetric correction procedure for light refraction effects at a two-medium boundary. *Photogrammetric Engineering and Remote Sensing, 74(9)*, 1129-1136.

Nazeer, M., Nichol, J.E., and Yung, Y.K., 2014. Evaluation of atmospheric correction models and Landsat surface reflectance product in an urban coastal environment. *International Journal of Remote Sensing, 35(16)*, 6271-6291.

Pairaud, I., Lyard, F., Auclair, F., Letellier, T., and Marsaleix, P., 2008. Dynamics of the semi-diurnal and quarter-diurnal internal tides in the Bay of Biscay. Part 1: Barotropic tides. *Continental Shelf Research, 28*, 1294-1315.

Potuckova, M., 2004. Image matching and its applications in photogrammetry. *Aalborg: Institut for Samfundsudvikling og Planlægning, Aalborg Universitet.*

Rinner, K., 1969. Problems of two-medium photogrammetry. *Photogrammetric Engineering, 35(2)*, 275-282.

Rupnik, E., Pierrot Deselligny, M., Delorme, A., and Klinger, Y., 2016. Refined satellite image orientation in the free open-source photogrammetric tools APERO/MicMac. *ISPRS Annals of the Photogrammetry, Remote Sensing, and Spatial Information Sciences, 3(1)*, 83-90.

Stumpf, R.P., Holderied, K., and Sinclair, M., 2003. Determination of water depth with high-resolution satellite imagery over variable bottom types. *Limnology and Oceanography, 47(1)*, 547-556.

Schenk, T., 2005. Introduction to Photogrammetry. *Department of Civil and Environmental Engineering and Geodetic Science, Ohio State University, GS400.02.*

Su, H., Liu, H., Wang, L., Filippi, A.M., Heyman, W.D., and Beck, R.A., 2014. Geographically adaptive inversion model for improvising bathymetric retrieval from satellite multispectral imagery. *IEEE Transactions on Geoscience and Remote Sensing, 52(1)*, 465-476.

Vajtäme, E., and Kutser, T., 2007. Mapping bottom type and water depth in shallow coastal waters with satellite remote sensing. *Journal of Coastal Research, 50*, 185-189.

Vinayaraj, P., Raghavan, V., and Masumoto, S., 2016. Satellite-derived bathymetry using adaptive geographically weighted regression model. *Marine Geodesy, 39(6)*, 458-478.

Witmer, J.D., Pe'eri, S., Imahori, G., Wozencraft, J.M., and Aslaksen, M.L., 2016. Using JALBTCX-USACE airborne lidar bathymetry to update coastal bathymetry on NOAA nautical charts. *Canadian Hydrographic Conference, May 16-19, Halifax.*

2.9 Author Contributions

Matus Hodul conducted the research for, and wrote this paper. Stephen Bird, Anders Knudby, and René Chénier contributed advice and knowledge, as well as assistance with editing.

Chapter 3

Photogrammetric Bathymetry for the Canadian Arctic

Matúš Hodúl [a,b], René Chénier [b], Marc-André Faucher [b], Ryan Ahola [b], Anders Knudby [a], Stephen Bird

[a] Department of Geography, Environment, and Geomatics. University of Ottawa, Ottawa,ON, Canada
[b] Canadian Hydrographic Service. Ottawa, ON, Canada

Abstract

Remote sensing techniques are becoming common in the estimation of bathymetry for the purpose of navigational charting through a process known as Satellite Derived Bathymetry (SDB). Most SDB techniques currently used by hydrographic offices employ an empirical approach, which requires the use of *in-situ* training data to calibrate a relationship between spectral information and coincident depths. Under a Government Related Initiatives Program (GRIP) with the Canadian Space Agency (CSA), the Canadian Hydrographic Service (CHS) is conducting research into these and alternative SDB approaches. This paper reports on a multi-site test of an alternative SDB method which uses photogrammetry to extract depths from stereo WorldView-2 imagery. In areas with a highly heterogeneous seafloor, the empirical approach faces difficulties in establishing the relationship between colour and depth, while the photogrammetric approach uses the contrasting seafloor features for feature triangulation. Additionally, the photogrammetric method may be applied in areas with no previous *in-situ* survey data, where the empirical approach would not be useful. Five study areas in Nunavut, Canada were selected to test the robustness of the method in different environments and under different imaging conditions. Study areas were (with resulting RMSE/Bias given in metres): Coral Harbour (0.78/-0.32), Cambridge Bay (1.16/-0.08), Queen Maud Gulf (0.97/0.13), Arviat (1.02/0.13), and Frobisher Bay, where extraction largely failed due to environmental conditions. Accuracies demonstrated in this study are very similar to those seen using the established empirical approach, suggesting that these two methods may be used in conjunction, each applied to the regions where they are better suited.

3.1 Introduction

As ice coverage in the Canadian Arctic declines, there has been a rapid increase in shipping traffic through the region, whose waters are both dangerous and remote (Pizzolato et al 2016). Though the Canadian Hydrographic Service (CHS) has charts for the entire country, there remain gaps in survey coverage in the Arctic, and most existing surveys in these regions are not to modern standards. In an effort to fullfil its mandate to provide bathymetric data for all Canadian waters, CHS with funding from a Government Related Initiatives Program (GRIP) with the Canadian Space Agency (CSA), has turned to remote sensing and Satellite Derived Bathymetry (SDB) in an attempt to generate bathymetric data over shallow waters.

Currently, most charting applications of SDB use some variation of an empirical spectral ratio approach introduced by Stumpf et al. (2003), which creates an empirical regression between upwelling spectral radiance and depth. Such methods have been used by the National Oceanic and Atmospheric Administration (NOAA), the French Service Hydrographique et Océanographique de la Marine (SHOM) and the United Kingdom Hydrographic Office (UKHO) to update production charts with SDB data (Mavraeidopoulos et al. 2017). SHOM has been using SPOT imagery for this purpose since 1988, and now routinely develops charts using such data (Laporte et al. 2015). UKHO has suggested that these methods are capable of producing data accurate to the CATegory Zone Of Confidence (CATZOC) C level, suitable for identifying navigational hazards or updating shoal positions (UKHO 2015).

Such advancements are encouraging for the acceptance of SDB application to navigational charting; however, empirical methods have assumptions and requirements which limit their application. Chiefly, the methods rely on *in-situ* bathymetric data for calibration of the band-ratio/depth regression, meaning they may not be used in unsurveyed waters, rapidly changing environments, or areas which cannot be safely accessed by survey vessels.

Additionally, empirical methods make assumptions regarding the scene-wide applicability of the modelled regression. Early, single band SDB approaches made the tenuous assumptions that both bottom type and water quality were homogenous across an area of interest (Polcyn et al. 1970), necessary for the application of a single regression model. The Stumpf et al. (2003) band ratio algorithm was meant to work in heterogeneous bottom environments; however, in most cases its performance in such environments is not satisfactory (Su et al. 2014). Instead a complicated locally-adapted model must be applied for each bottom type (Vinayaraj et al. 2016), which places even greater requirements on calibration data.

The photogrammetric technique is able to avoid these two limitations by relying on image geometry and feature matching rather than an empirical relationship between depth and colour. The known location and orientation of imaging sensors is used to triangulate features in stereo imagery (Figure 3.1). Satellite sensor position and orientation is measured during each image exposure using onboard GPS, gyros, and star trackers (Grodecki and Dial 2003), and is approximated by a Rational Function Model (RFM) during feature triangulation. Tie points, prominent objects within the scene that are identified on both images, may be used to further refine the RFM, improving positioning accuracy (Hobi and Ginzler 2012). Ground surface features are then matched between images using a variety of possible algorithms, by finding points or edges which are common to both stereo images (Potuckova 2004). These triangulated feature positions and elevations are used to build a Digital Elevation Model (DEM).

Through-water photogrammetry presents a greater challenge, in part due to the effects of light refraction at the air-water boundary, requiring a refraction correction. Hodul et al. (2018) presented a proof-of-concept for satellite derived photogrammetric bathymetry using WorldView-2 stereo imagery, where a vertical accuracy of 1.178 m and a vertical bias of 0.031 m were achieved for a single stereo image pair in the Canadian

Arctic. This paper tests the approach with five additional WorldView pairs across Canada, investigating the robustness of the approach across varying bottom types and sea surface conditions.

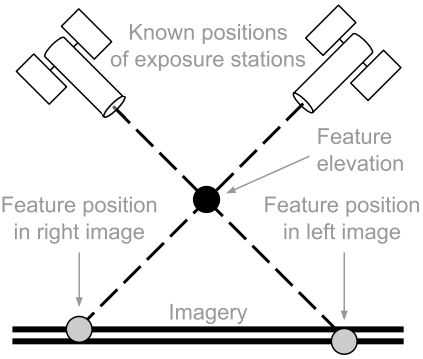

Figure 3.1: A simplified diagram of photogrammetric triangulation. The apparent displacement of a point feature between the two images, parallax, can be used in conjunction with the known position and orientation of the exposure station (satellite) at each exposure to derive the position and elevation of that feature.

3.2 Study Areas and Data

Five study areas across the Canadian Arctic were chosen as representative examples of Canadian arctic nearshore Arctic environments in which the satellite derived photogrammetric bathymetry technique was tested. Figure 3.2 shows the five study areas: *Coral Harbour, Cambridge Bay, Queen Maud Gulf, Arviat*, and *Frobisher Bay*. For each area, a WorldView-2 (WorldView-3 for *Queen Maud Gulf*) stereo pair was acquired, metadata for which are show in Table 3.1. The imagery was acquired in *Stereo Ortho-Ready 2A* format, and the 2 m multispectral imagery was used in all processing steps. Imagery was acquired by CHS with funds from a Government Related Initiatives Program (GRIP) of the Canadian Space Agency (CSA).

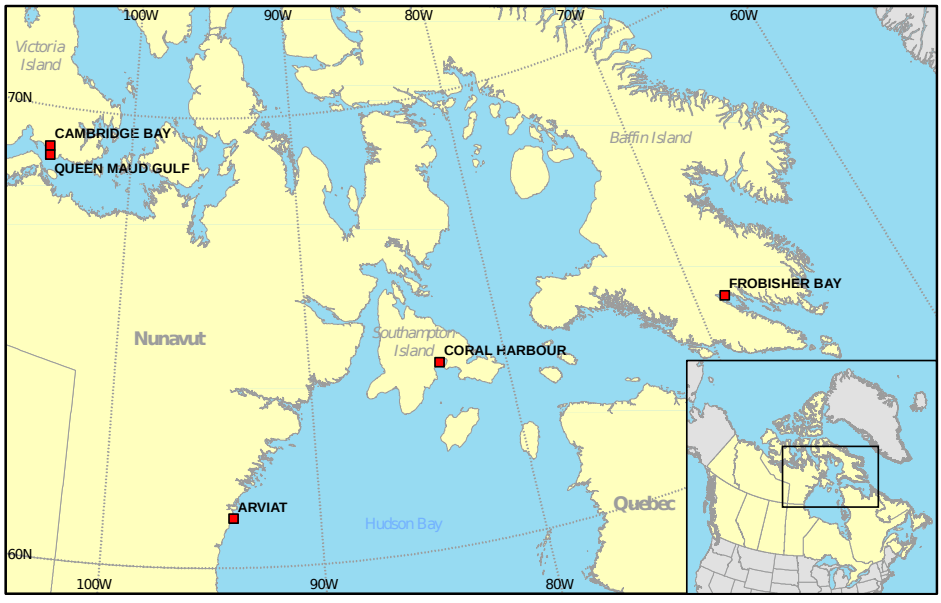

Figure 3.2: Location of the five study areas. Red squares do not represent exact imagery extents. *Cambridge Bay* and *Queen Maud Gulf* are adjacent and overlap by about 2.3 km. Contains information licensed under the Open Government Licence – Canada.

Table 3.1: Summary of Stereo pairs used for each study site, given as DigitalGlobe catalog IDs. Angles given in degrees, dates given in yyyy-mm-dd, and times given in UTC. All information in this table was obtained from metadata for each image.

Coral Harbour	103001001A9F7500	1030010019771700
Acquisition Date and Time	2012-07-18 17:34:27	2012-07-18 17:35:37
Mean Off-Nadir View Angle	0.5	30.7
Mean Cross-Track View Angle	0.5	-0.5
Mean In-Track View Angle	-0.2	-30.6
Cambridge Bay	1030010048084400	103001004A31F700
Acquisition Date and Time	2015-09-20 18:37:36	2015-09-20 18:38:47
Mean Off-Nadir View Angle	28	16.2
Mean Cross-Track View Angle	14.7	14.1
Mean In-Track View Angle	24	-8
Queen Maud Gulf	104001002ECD9D00	104001002F4BE000
Acquisition Date and Time	2017-07-11 19:22:08	2017-07-11 19:23:15
Mean Off-Nadir View Angle	13.7	27.7
Mean Cross-Track View Angle	-5.5	-6.4
Mean In-Track View Angle	12.5	-27
Arviat	103001000C58CA00	103001000C0EF600
Acquisition Date and Time	2011-07-22 17:47:31	2011-07-22 17:48:44
Mean Off-Nadir View Angle	17.1	34.2
Mean Cross-Track View Angle	17.1	15.7
Mean In-Track View Angle	-0.8	-30.8
Frobisher Bay	103001005975FA00	103001005A9A7F00
Acquisition Date and Time	2016-08-07 15:45:07	2016-08-07 15:46:13
Mean Off-Nadir View Angle	25.1	27
Mean Cross-Track View Angle	22.2	21.3
Mean In-Track View Angle	12	-17.1

CHS bathymetric survey data was used for validation of estimated bathymetry. Vertical datums for these data are represented as Chart Datum, defined as the mean lower low water at large tide for each area (DFO 2016).

3.3 Method

This paper reports on a multi-site test of the robustness of the photogrammetric bathymetry method proposed by Hodul et al. (2018), and reproduces the method exactly. It proceeds in four main steps, illustrated in Figure 3.3: A) Photogrammetric extraction, B) waterline height extraction, C) refraction correction, and D) tidal reduction. A brief description of each step is provided below, while a detailed description may be found in Hodul et al. (2018).

3.3.1 A. Photogrammetric Extraction

A standard photogrammetric extraction is performed on the green band of the stereo pair using image-provided Rational Polynomial Coefficients (RPCs) and automatically generated, land-based tie points. In this paper, PCI Geomatica was chosen for photogrammetric extraction; however any professional-level photogrammetry software may be used. The green band is used because, for these five study sites, seafloor features at a broad range of depths are most consistently visible and sharply defined at this wavelength. Extracted points were thresholded such that points with a correlation score lower than 70% were removed.

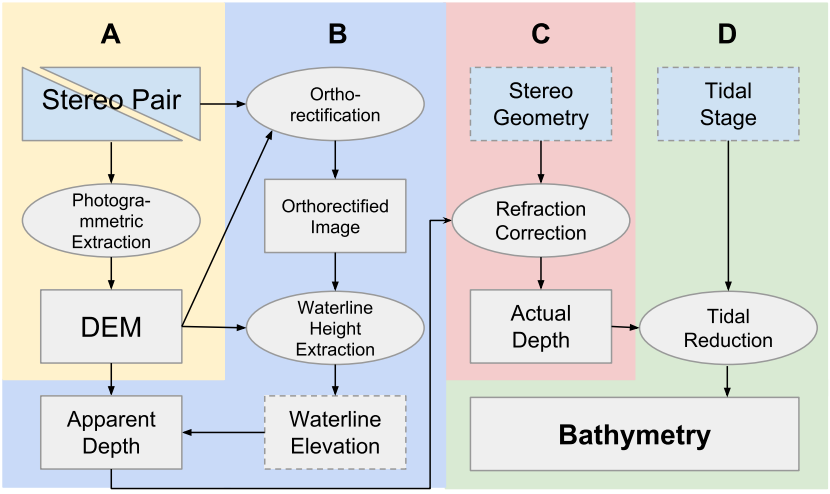

Figure 3.3: Illustrated outline of the four-step method developed by Hodul et al. (2018) for satellite derived photogrammetric bathymetry. A) Standard stereo extraction. B) Waterline height extraction. C) Refraction correction. D) Tidal reduction.

3.3.2 B. Waterline Height Extraction

To convert the output DEM values from elevation above ellipsoid to apparent water depth, the ellipsoidal elevation of the coastline is determined using a thresholded near-infrared band (Band 8), with elevations extracted at water boundaries. The mode of these values, binned into 0.1 m intervals, is used as the waterline height. This is then subtracted from the DEM, and the resulting values are inverted to represent apparent depth rather than negative elevation.

3.3.3 C. Refraction Correction

Apparent depths h_a, which are underestimated due to the effects of refraction at the air-water boundary, are converted into actual water depths h (at the time of image acquisition) using a refraction correction adapted from Murase et al. (2008), calculated as

$$h = \frac{\tan r_A \cos\theta_A + \tan r_B \cos\theta_B}{\tan i_A \cos\theta_A + \tan i_B \cos\theta_B} * h_A \tag{3.1}$$

where r is the off-nadir incidence angle for left and right stereo exposures A and B,

$$i = \sin^{-1}\left(\frac{\sin r}{n}\right) \tag{3.2}$$

$$\theta = \tan^{-1}\left(\frac{\tan\delta_c}{\tan\delta_i}\right) \tag{3.3}$$

where δ_c and δ_i are the cross-track and in-track components of the incidence angle, and n is the refractive index of water (1.34). Incidence angles are calculated calculated from view angles (Table 3.1) as

$$\beta = \sin^{-1}\left(\frac{R+H}{R}\sin\alpha\right) \tag{3.4}$$

where α is the view angle, β is the incidence angle, H is the orbital altitude of the sensor, and R is the Earth's radius.

3.3.4 D. Tidal Reduction

Finally, a tidal reduction is performed to bring depths to chart datum by subtracting tidal stage from actual depth values. Tidal stage at the time of image acquisition is modelled at each study area using the Toulouse Unstructured Grid Ocean Model (Pairaud et al. 2008; Collins et al. 2011).

3.3.5 Bathymetry Post Processing

Objects on the sea surface which are correlated at the feature matching phase of the photogrammetric extraction will result in elevations which do not represent bathymetry. A stationary object will have an elevation identical to the waterline, however most objects (for example boats, animals, debris, and ice) will not be stationary. Their movement will appear to the photogrammetric algorithm as additional parallax, resulting in the object being assigned an erroneous elevation based on the direction and magnitude of its movement. Stationary and moving sea surface objects manually identified in the imagery, and the corresponding pixels in the DEM are removed.

3.4 Results

Table 3.2 presents the results of the waterline height calculation, the refraction correction factor, and the modelled tidal stage for each study area. Resulting bathymetric surfaces for each study area are discussed below.

Table 3.2: Results of calculations for waterline height (m above ellipsoid), refraction correction factor, and tidal stage (m above chart datum).

Study Area	Waterline Height	Refraction Factor	Tidal Stage
Coral Harbour	-34.3	1.47689	2.68
Cambridge Bay	-32.8	1.43076	0.48
Queen Maud Gulf	-30.3	1.41602	0.85
Arviat	-50.4	1.51980	3.09
Frobisher Bay	-5.6	1.43365	10.03

3.4.1 Coral Harbour

Figure 3.4 shows the complete, post-processed bathymetric surface for the *Coral Harbour* study site. Minimal post-processing was needed, as the scene contained exceptionally smooth water and very few water-surface objects. DEM data in the eastern section of the image was removed due to cloud cover. DEM extraction resulted in nearly complete coverage in optically shallow areas, with the exception of some locations in the northwestern quadrant of the image, where the seafloor contained too few features for correlation. The Figure 3.4 insets demonstrates the need for such features in the extraction process, showing successful extraction in the light/dark speckled regions, but no successful extraction in the smooth, sandy regions.

Evaluation of the results against the ship-based CHS survey (Figure 3.5) showed that there was a slight underestimation of depths, resulting in a bias of -0.32 m. The Root Mean Square Error (RMSE) was found to be 0.78 m

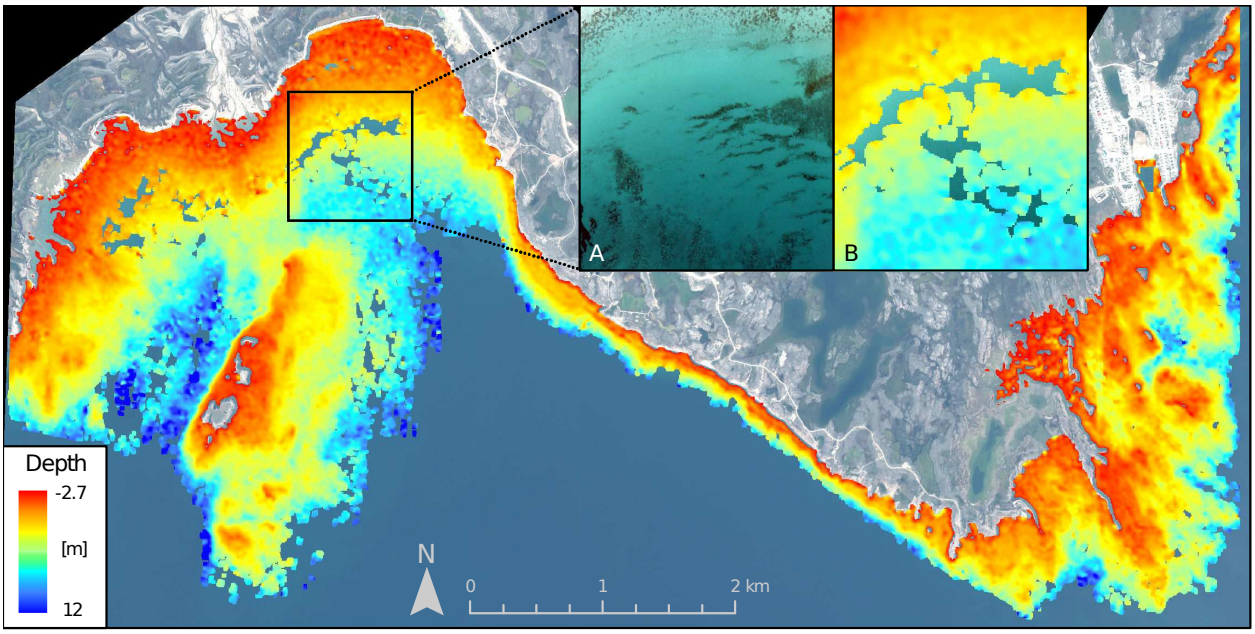

Figure 3.4: Photogrammetrically extracted bathymetric surface for the *Coral Harbour* study area, overlaid on a true-colour image of one of the stereo pairs (103001001A9F7500). The insets show A) an area with both sandy, featureless bottom and heterogeneous bottom; and B) the corresponding bathymetric surface. These illustrate how feature matching can fail in featureless areas, which can leave 'holes' in the resulting bathymetry. Imagery ©2012, DigitalGlobe, Inc.

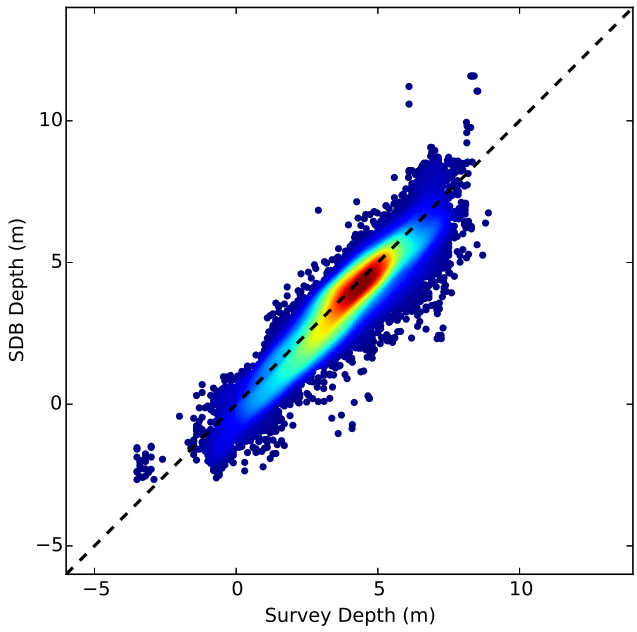

Figure 3.5: Validation scatter plot of the *Coral Harbour* bathymetry, against 21,063 CHS survey points. Dashed line indicates x=y, and colour ramp indicates point density with red as most dense.

3.4.2 Cambridge Bay

The *Cambridge Bay* extraction (Figure 3.6) yielded better results in areas where the bottom contained many contrasting features (Figure 3.6, inset A), which made up most of the shallow portions of the bay. In the

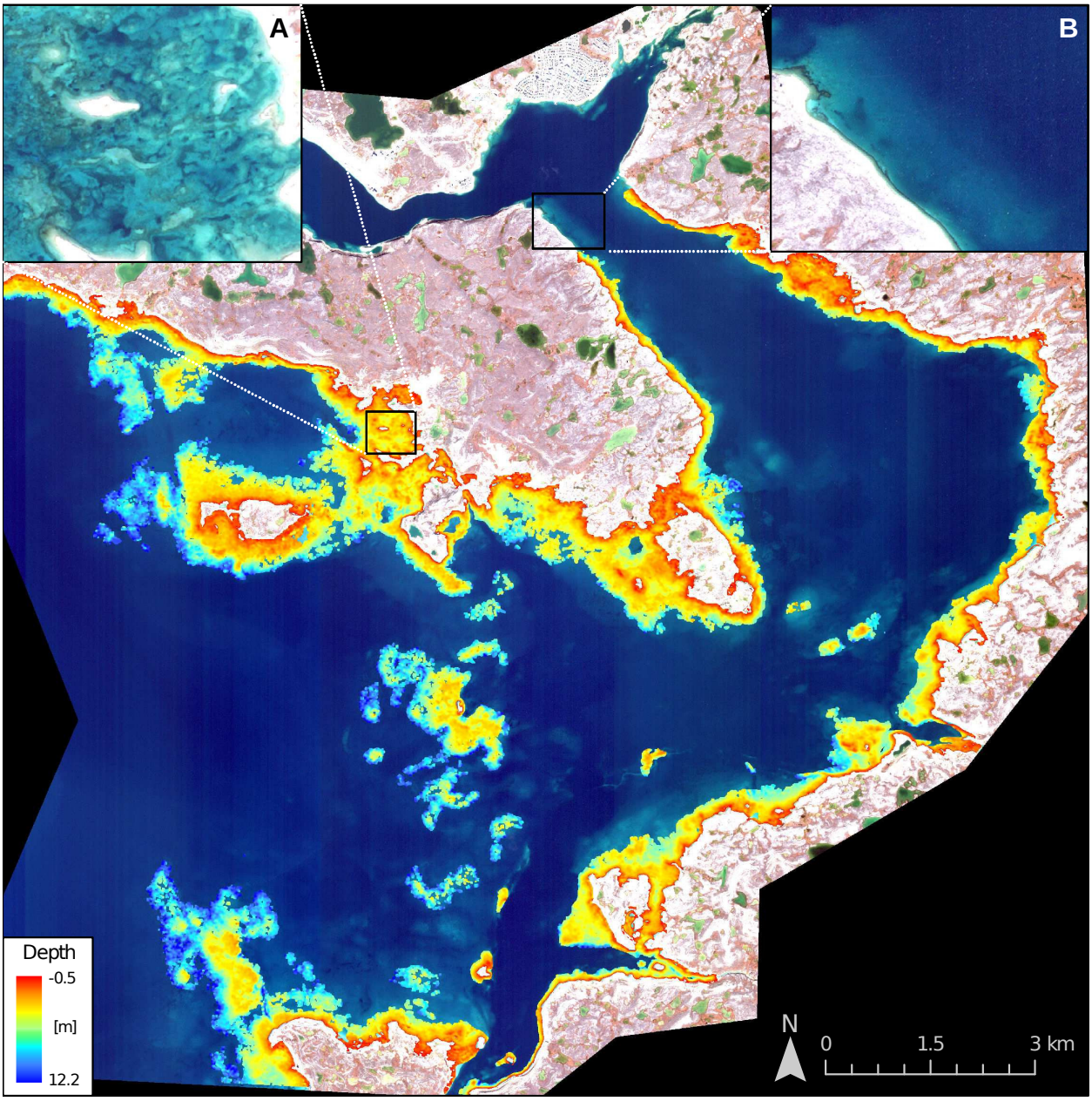

Figure 3.6: Photogrammetrically extracted bathymetric surface for the *Cambridge Bay* study area, overlaid on a true-colour image of one of the stereo pairs (1030010048084400). The two insets demonstrate the difference between a highly heterogeneous surface with small contrasting features (inset A), and a smooth, sandy, featureless surface (inset B). The difference in surface types resulted in the presence or absence of well estimated depths in these areas. Imagery ©2015, DigitalGlobe, Inc.

northernmost parts of the bay, bottom type was consistently sandy and featureless (Figure 3.6, inset B). As a result, most matched features originated from the sea surface, and were removed in post-processing. Areas in the southern portion also recquired substantial post-processing to remove bathymetry values incorrectly estimated due to small pieces of ice on the water surface, typically about 1-4 pixels in size.

The validation scatterplot (Figure 3.7) shows that most points were vertically accurate to within a metre, though with some outliers, resulting in an RMSE of 1.16 m and a bias of -0.08 m.

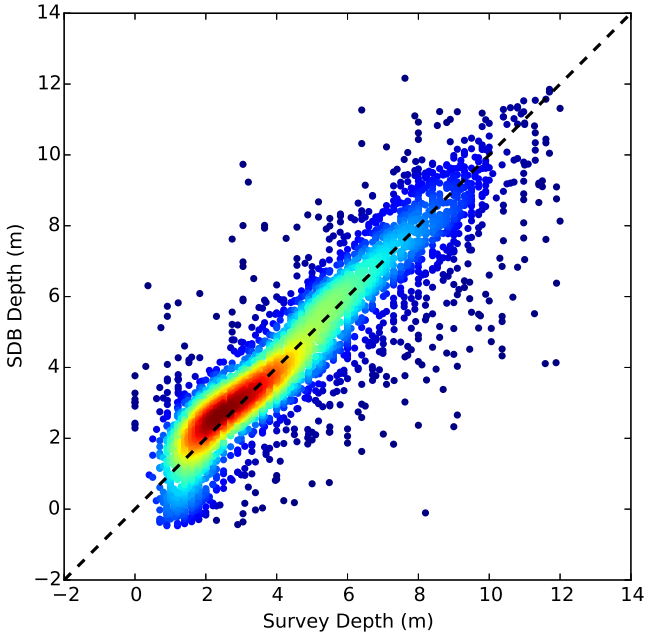

Figure 3.7: Validation scatter plot of the *Cambridge Bay* bathymetry, against 4103 CHS survey points. Dashed line indicates x=y, and colour ramp indicates point density with red as most dense.

3.4.3 Queen Maud Gulf

Queen Maud Gulf results show a nearly complete photogrammetric extraction in shallow areas (Figure 3.8).

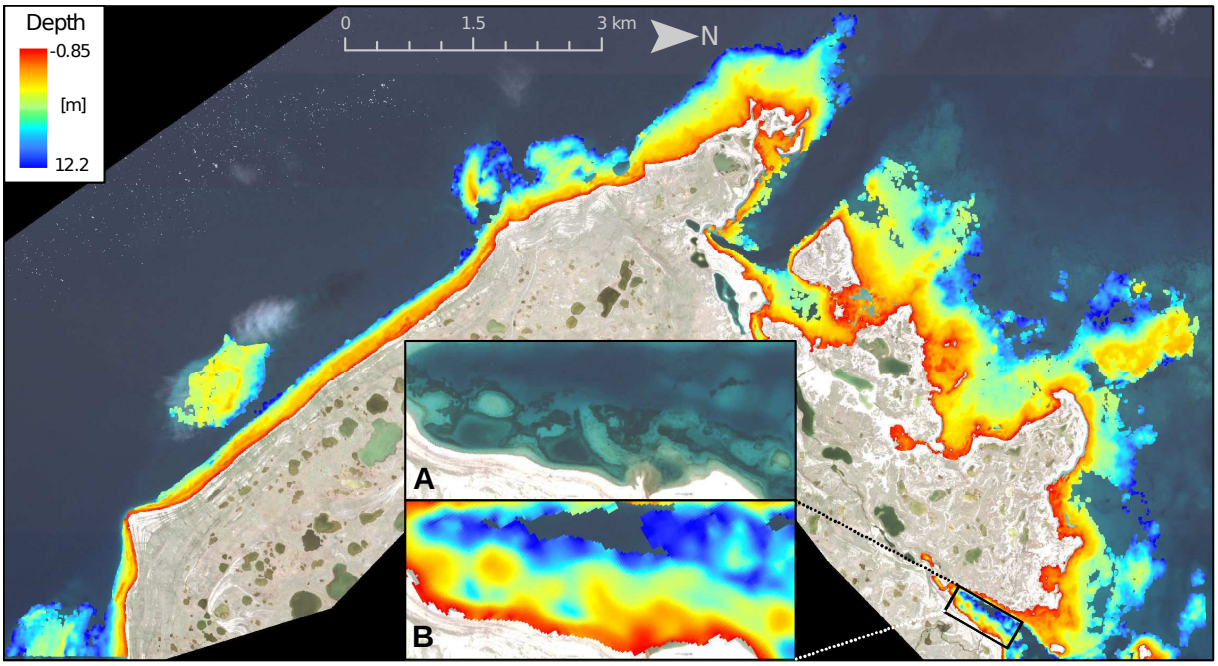

Figure 3.8: Photogrammetrically extracted bathymetric surface for the *Queen Maud Gulf* study area, overlaid on a true-colour image of one of the stereo pairs (104001002F4BE000). The insets show a particularly complicated area of bathymetry (A) which has been successfully mapped (B). Imagery ©2017, DigitalGlobe, Inc.

This scene contained a large amount of water surface objects in some areas, as well as some cloud cover. The ice chunks in the southwest (in Figure 3.8 this is towards the top left) did not affect extraction, as they were over optically deep water; however in the northern sections of the image (right), small floating ice pieces similar to those seen in *Cambridge Bay*, caused the extraction to fail, requiring post-processing of the extracted bathymetry. Figure 3.9 shows the scatter plot, with a bias of 0.13 m and an RMSE of 0.97 m.

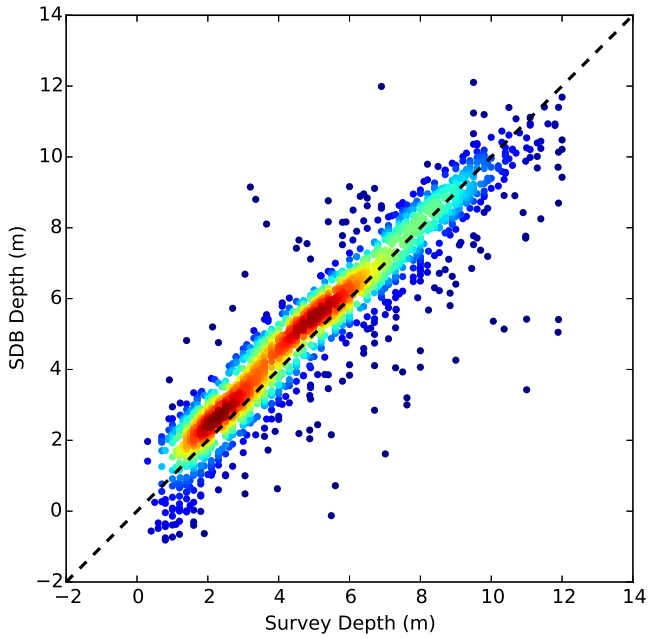

Figure 3.9: Validation scatter plot of the *Queen Maud Gulf* bathymetry, against 2063 CHS survey points. Dashed line indicates x=y, and colour ramp indicates point density with red as most dense.

3.4.4 Frobisher Bay

Much of the area in *Frobisher Bay* did not result in a good DEM extraction. The water in the shallow region near the community of Iqaluit contained suspended sediment, occluding the sea floor. Other shallow areas have a large amount of wave glint and other surface objects, which resulted in either poor DEM extraction or extreme errors in bathymetry (Figure 3.10). A glint correction (Hedley et al. 2005) was attempted, but sufficient glint in optically deep water was not present.

Some sheltered areas did appear to produce good DEM extraction such as the area shown in Figure 3.11. No survey depth data was available for this specific location.

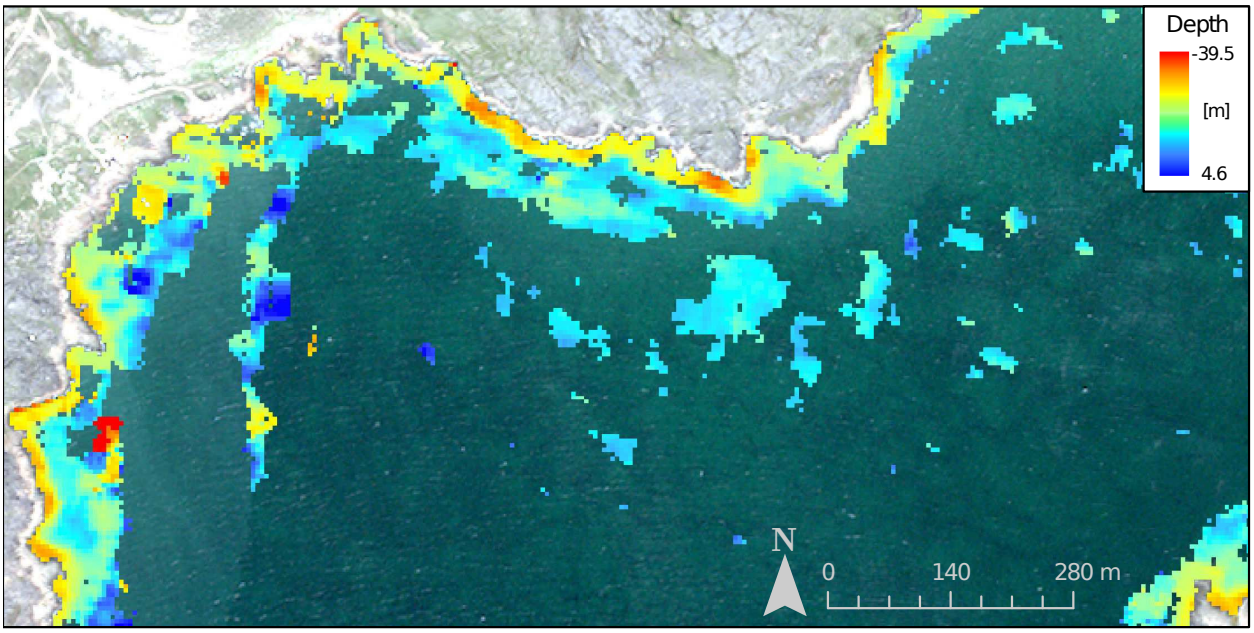

Figure 3.10: A section of the *Frobisher Bay* study area (image 103001005975FA00) , showing an area of shallow water with a heterogeneous bottom which should ordinarily result in excellent DEM extraction. However, due to the presence of wave glint, good DEM extraction is extremely patchy, with many major errors present. Imagery ©2016, DigitalGlobe, Inc.

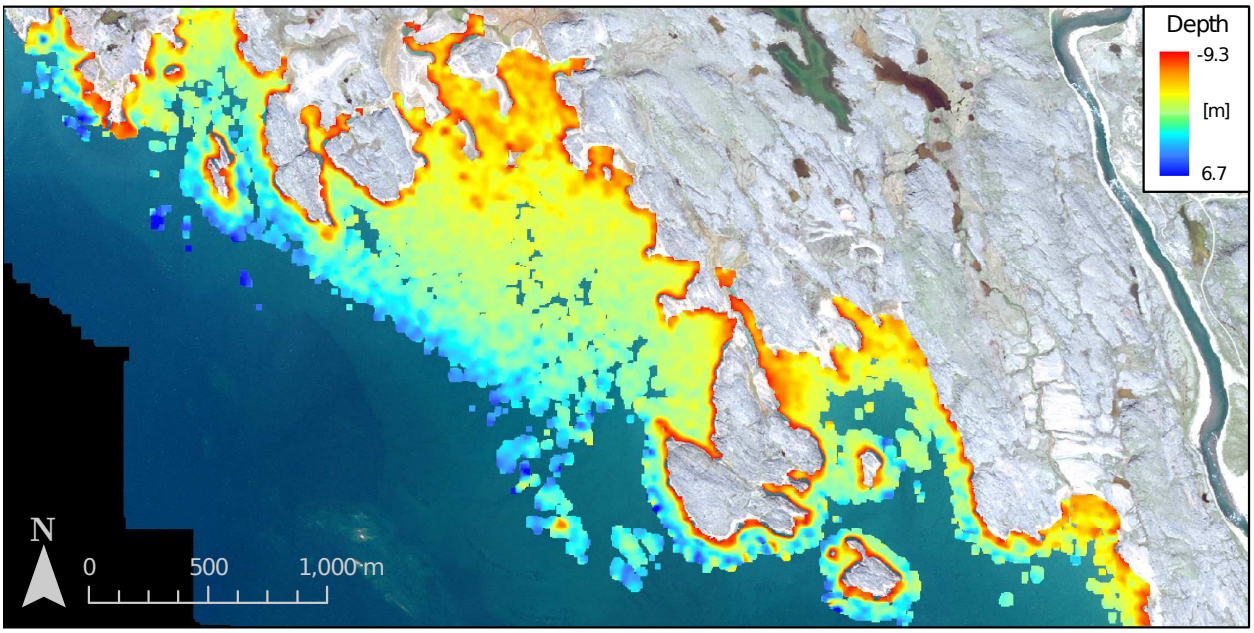

Figure 3.11: A section of the *Frobisher Bay* study area (image 103001005975FA00) , showing an area which was sheltered enough from waves, and thus glint, allowing for an improved DEM extraction. Imagery ©2016, DigitalGlobe, Inc.

3.4.5 Arviat

Bathymetry results in the *Arviat* study area were somewhat successful, although problems with the imagery resulted in the obvious striping seen in Figure 3.12.

This was likely caused by the extremely small parallax seen in the optically shallow areas of *Arviat*. Figure 3.13 illustrates the small parallax seen in *Arviat*, as compared to *Queen Maud Gulf* and *Coral Harbour*. Parallax displacement in *Arviat* is of a sub-pixel magnitude, while the other two sites have displacement on the order of tens of pixels. Such small topographically-generated parallax likely caused small geometric irregularities between the stripes to become a dominant source of parallax, which would otherwise be made negligible by the topographical parallax in other stereo pairs. These irregularities may be caused by jitter in the individual sensor components following the targeting motion of the platform, which is not accounted

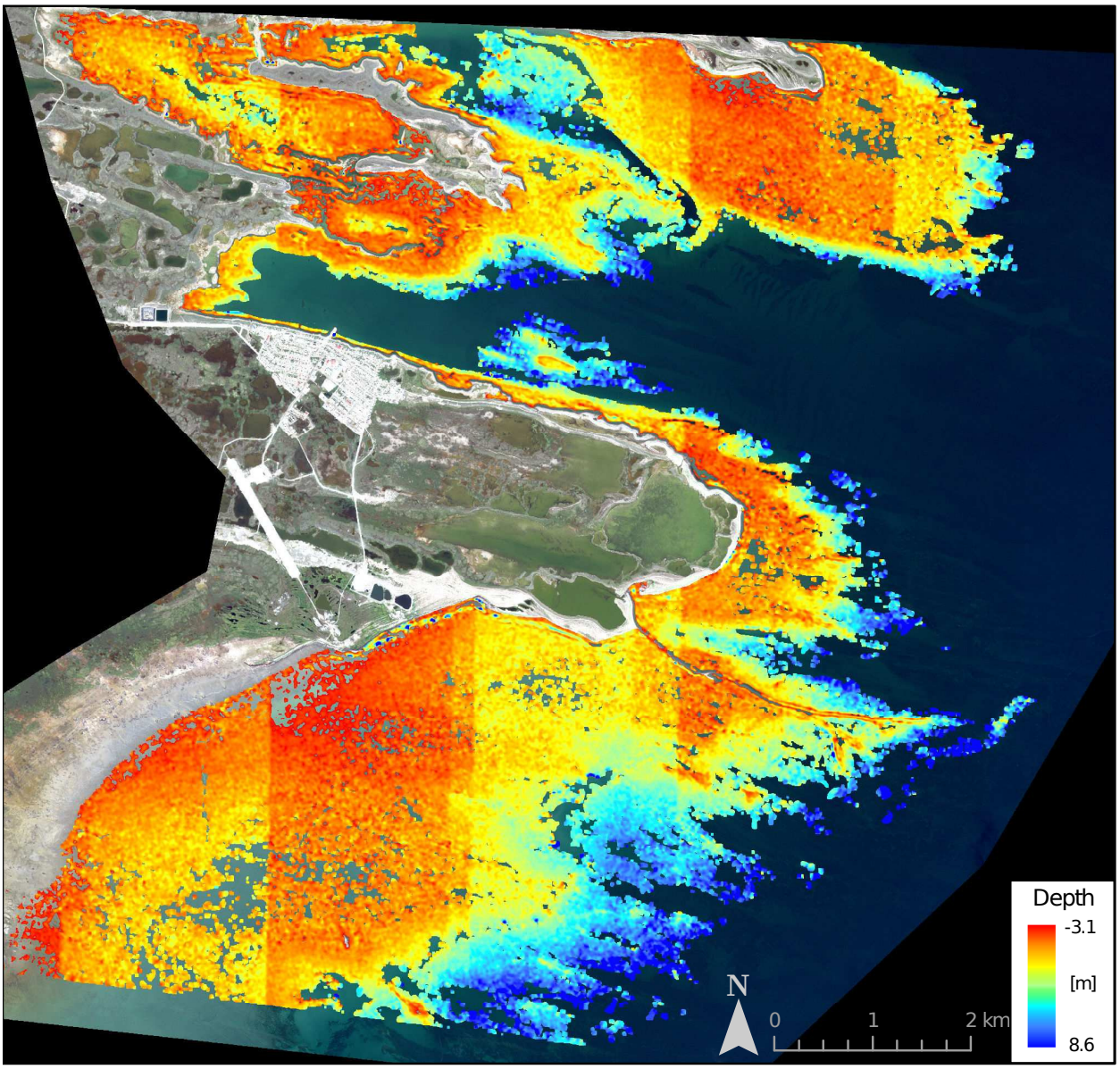

Figure 3.12: Photogrammetrically extracted bathymetric surface for the *Arviat* study area, overlaid on a true-colour image of one of the stereo pairs (103001000C58CA00). Imagery ©2011, DigitalGlobe, Inc.

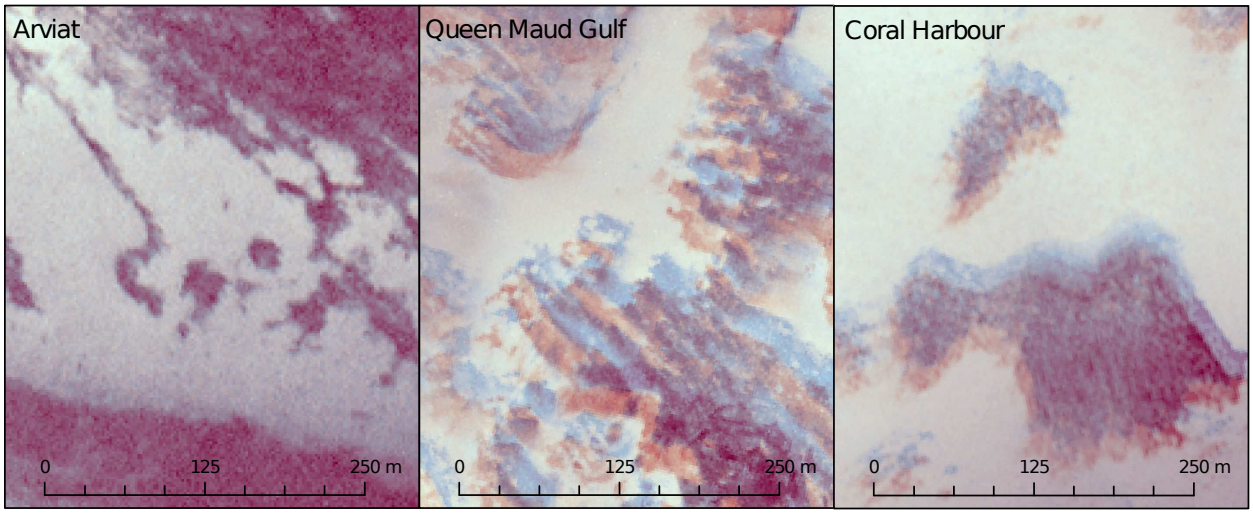

Figure 3.13: An illustration of the magnitude of parallax seen in *Arviat* (left), *Queen Maud Gulf* (centre), and *Coral Harbour* (right) study areas. Features were chosen to be of a similar type and size across the three areas, as well as at a similar depth (scale for all panels is identical). The images are constructed by showing the green band of each image in the stereo pair in a blue and red colour rendering respectively, making their displacement evident. Movement in *Arviat* is of a sub-pixel magnitude, while the other two sites have displacement on the order of tens of pixels. Imagery ©2011, DigitalGlobe, Inc.

for in the RPCs, causing geometric irregularities of around 10 cm in some cases (Jacobsen 2017).

Though the results in *Arviat* do not appear useful due to this geometry problem, the validation scatter plot still reveals the vertical bias and accuracy to be reasonably good (Figure 3.14), with an RMSE of 1.02 m and a bias of 0.13 m.

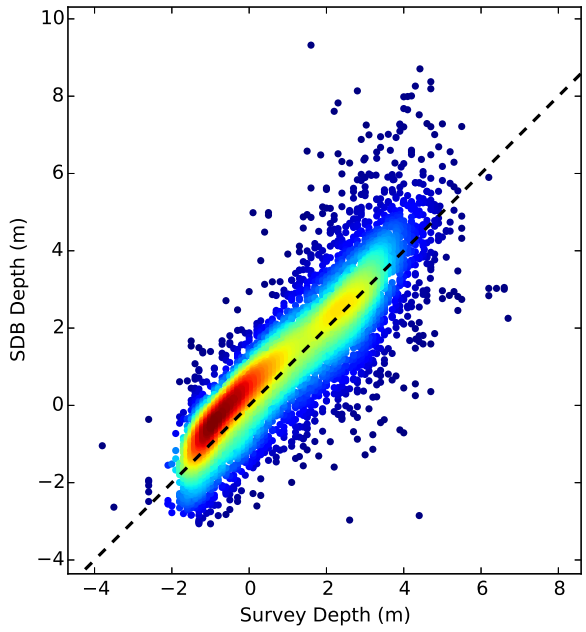

Figure 3.14: Validation scatter plot of the *Arviat* bathymetry, against 5936 CHS survey points. Dashed line indicates x=y, and colour ramp indicates point density with red as most dense.

3.5 Discussion

3.5.1 Environmental Considerations and Imagery Selection

A successful stereo bathymetric extraction relies on the quality of the stereo imagery used, as well as the suitability of the study area for feature matching. Aside from the typical SDB considerations of cloud cover and water clarity, there are two additional considerations specific to photogrammetric bathymetry: bottom type, which will define a site's suitability; and surface disturbances, which will influence the quality of feature extraction and refraction correction.

Bottom Type

The need for a heterogeneous seafloor containing relatively small, contrasting features was confirmed, particularly with results from *Coral Harbour* and *Cambridge Bay*. In both of these study areas, sections of the sea floor which contained no contrasting features, but rather a smooth sandy texture, produced incomplete or incorrect DEM extraction; details which are shown in the insets of Figures 3.4 and 3.5. Lack of heterogeneous bottom represents a fundamental limiting factor of the photogrammetry method; reducing its viability for regions which have smooth, featureless bottoms. Fortunately, this represents the type of environment where empirical methods work best, given adequate survey data. Thus, when assessing a site for its potential for SDB, the most appropriate method must be chosen based on bottom type. In areas such as Cambridge Bay where heterogeneous and homogeneous bottom types are present, each method can be applied to appropriate sections of the site, allowing for bathymetry estimates to be derived over a larger area than would otherwise be possible through application of only one SDB approach.

Surface Disturbances

A sea surface containing a great deal of visible waves, seen in the imagery as glint, is undesirable for two reasons: glint interfering with feature matching, and the assumptions made during refraction corrections.

Waves which have wavelengths on the order of a few pixels create glint which makes feature matching of seafloor objects difficult, reducing the number of good matches, and leading to a DEM containing data gaps. This was observed most clearly in Figure 3.10. A glint correction may be able to resolve bottom visibility issues, but would not resolve geometric irregularities in feature positions caused by the refraction, which will affect the ease of feature matching. In addition, the waves themselves are occasionally correlated between images, resulting in the significant errors in DEM extraction which need to be manually edited out of the resulting bathymetry.

The geometry of the refraction correction procedure assumes a perfectly planar surface at the air-water boundary (Rinner 1969). Small waves, on the order of a few pixels in length, have been found to have a negligible effect (Fryer and Kniest 1985). However, large waves would produce errors in the refraction correction. Thus, when selecting imagery, it is best to choose pairs which contain smooth water.

3.5.2 Comparison to Empirical SDB Accuracy

Most literature on empirical SDB approaches has tested the method in ideal locations, particularly those at low latitudes (thus high sun elevations), with exceptionally clear water. Typical vertical accuracies are around 1 m using a variety of sensors (Jawak and Luis 2015; Jégat et al. 2016; Said et al. 2017), reaching to 0.89 m in ideal conditions (Pacheo et al. 2015).

However, such ideal conditions rarely occur in the Canadian Arctic. CHS has conducted some preliminary research in the Canadian Arctic (Chénier et al. 2016), at the *Cambridge Bay* study area using a different WorldView-2 image. Their best results were found using a log ratio of the coastal and yellow bands, showing a Mean Absolute Error (MAE) of 1.3 m in a 0-10 m depth range. Vertical accuracy results demonstrated in this paper as well as in Hodul et al. (2018), ranging from 0.78 to 1.16 m RMSE, show the photogrammetric SDB method to have vertical accuracies similar to the empirical method. For instance, in the *Cambridge Bay* study area, the photogrammetry approach yields an MAE of 0.80 m, compared to 1.3 m for the empirical approach from Chénier et al. (2016).

3.5.3 Application to Charting

The International Hydrographic Organization (IHO) classifies bathymetric surveys into orders based on their horizontal and vertical accuracy (Table 3.3). With a horizontal accuracy of about 3.5 m (CE90, DigitalGlobe 2016), and a vertical accuracy of 0.78-1.16 m, the photogrammetric method could, in ideal circumstances, constitute a survey of *at best* Order 2; however, the data is likely better classified as Order 3.

CHS chart 7750, encompassing both *Cambridge Bay* and *Queen Maud Gulf* study areas, can be used as an example of the potential for the method to aid in nearshore charting. One key benefit of the photogrammetric bathymetry method, over that of the empirical SDB method, is that it does not rely on in-situ survey data for any step in the process, allowing for its use in otherwise uncharted regions. Figure 3.15 shows an uncharted area which would be difficult to accurately map using empirical methods due to the lack of training data for model fitting. Using the photogrammetric technique, sections with depths less than about 12 m have been fully mapped; the size, position, and depth of known shoals may be updated (annotations A and B), or new shoals may be discovered (annotation C).

The second benefit of the photogrammetric method is its applicability in areas containing heterogeneous sea floor. Figure 3.16 shows an area of the *Cambridge Bay* study area which would be difficult to map using an empirical approach, because each type of substrate would need to be represented by an individual

Table 3.3: A simplified description of IHO Standards for Hydrographic Surveys (IHO 2008). Vertical accuracy is found as $\Delta h = \sqrt{\pm(a^2 + (bh)^2)}$. CHS uses this system for classifying its surveys (CHS 2013), with the addition of Exclusive and 3rd order, also shown below.

ORDER	Typical Areas	Horizontal Accuracy	Depth Accuracy
Exclusive	Shallow water in Harbours, berthing areas, and associated critical channels with minimum under-keel clearances or engineering surveys	1 m	a = 0.15 m b = 0.0075
Special	Harbours, berthing areas, and associated critical channels with minimum under-keel clearances	2 m	a = 0.25 m b = 0.0075
1A	Areas shallower than 100 metres where under-keel clearance is less critical but features of concern to surface shipping may exist.	5 m + 5% of depth	a = 0.5 m b = 0.013
1B	Areas shallower than 100 metres where under-keel clearance is not considered to be an issue for the type of surface shipping expected to transit the area.	5 m + 5% of depth	a = 0.5 m b = 0.013
2	Areas generally deeper than 100 metres where a general description of the sea floor is considered adequate.	20 m + 10% of depth	a = 1.0 m b = 0.023
3 (Impercise)	All areas where the accuracies do not meet the requirements of the previous orders	>20 m + 10% of depth	a = 1.0 m b = 0.023

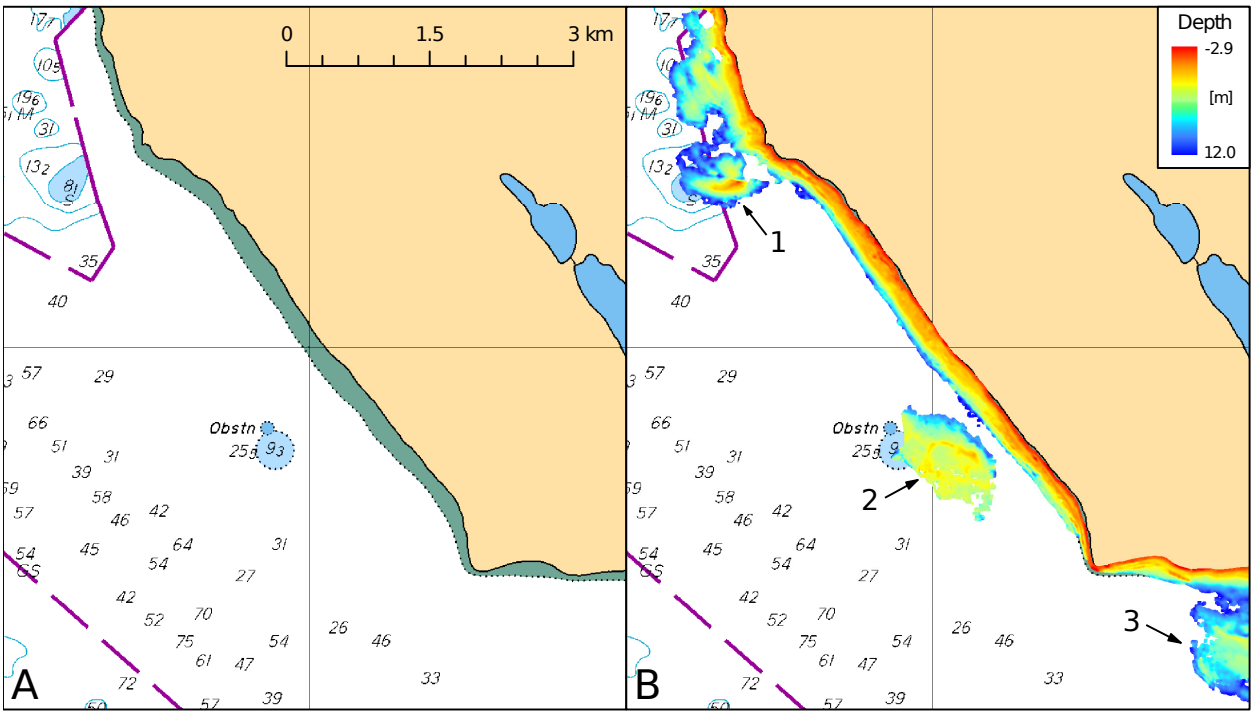

Figure 3.15: A section of the CHS chart 7750 showing a section of the coastline in Queen Maud Gulf (panel A), with the bathymetry data developed for the *Queen Maud Gulf* study area overlaid (panel B). The position, size, and depth of three shoals are revealed in an area with limited survey coverage. The complete size, position and depth of known shoals may be updated (annotations 1 and 2), and new shoals may be discovered (3). The right edge of the panels coincides with the easternmost extent of the imagery, so only a small portion of the shoal on the bottom right was mapped. The graticule in the centre of the chart indicates 68°55' N, 105°10' W; charted depths given in meters.

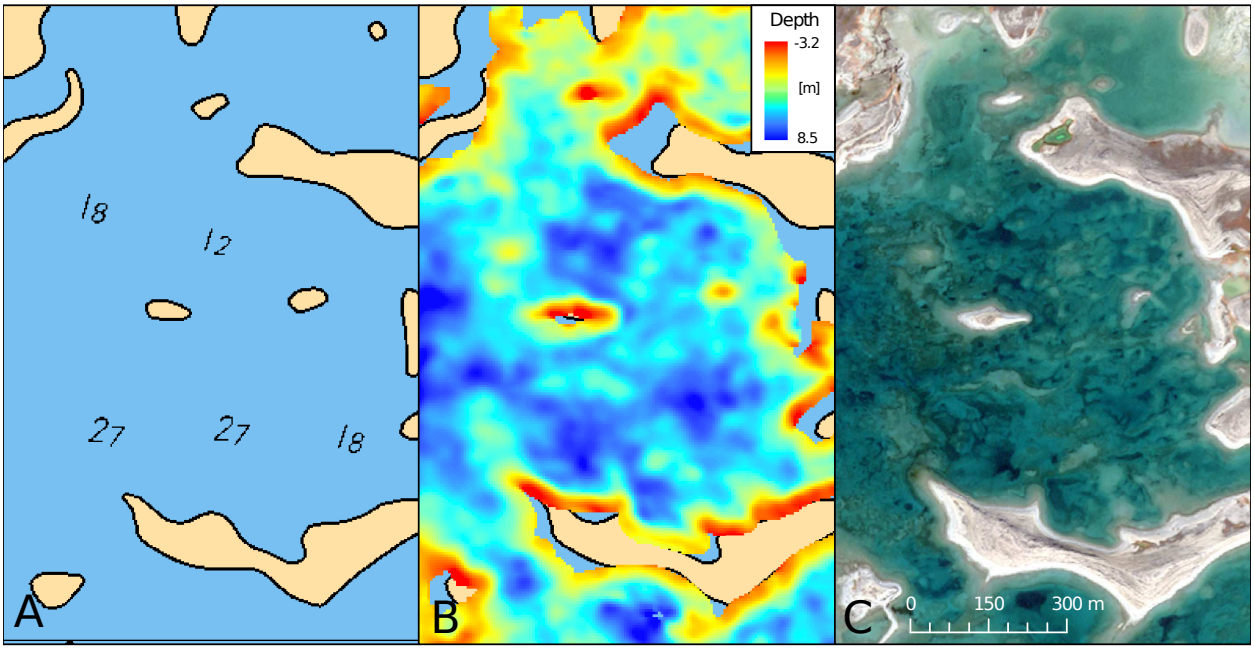

Figure 3.16: A section of the CHS chart 7750 showing Cambridge Bay (A), with the overlain bathymetry data developed for the *Cambridge Bay* study area (B), and a true colour image (C). Imagery ©2015, DigitalGlobe, Inc.

model. However, the photogrammetric method excels in these sorts of environments, allowing for a complete bathymetric surface to be extracted. In this case, this kind of data may allow for contour lines to be added to areas of CHS Chart 7750 where only single depth soundings are currently displayed.

3.6 Conclusion

The photogrammetric SDB technique proposed by Hodul et al. (2018) has been applied to five stereo pairs acquired in the Canadian Arctic in order to test the robustness of the method across sites at different latitudes and with different seafloor types and sea surface conditions. The method was shown to have a vertical accuracy of between 0.78 m and 1.16 m RMSE, to a depth of about 12 m, depending on seafloor type and sea surface conditions. It was observed that the seafloor should ideally contain small, contrasting features, to allow for appropriate triangulation during the photogrammetry process. It was also found that the sea surface should be as smooth as possible at the time of image acquisition to prevent glint and to maintain assumptions made during refraction correction. The vertical accuracy achieved using this method is similar to or better than that of the established empirical SDB methods currently in use by hydrographic offices for navigational charting, suggesting that it may be used in conjunction with such methods where lack of training data or a heterogeneous seafloor type make the empirical approach unfeasible.

3.7 Acknowledgments

This research has been conducted by the Canadian Hydrographic Service (CHS), and was made possible thanks to financial support by the Canadian Space Agency (CSA) through a Government Related Initiative Program (GRIP) project.

3.8 References

Chénier, R., Faucher, M.A., Ahola, R., Jiao, X., and Tardif, L., 2016. Remote sensing approach for updating CHS charts. *Canadian Hydrographic Conference, May 16-19, Halifax.*

CHS 2013. Standards for Hydrographic Surveys. *Canadian Hydrographic Service*

Collins, A.K., Hannah, C.G., and Greenberg, D., 2011. Validation of a high resolution modelling system for tides in the canadian arctic archipelago. *Canadian Technical Report of Hydrography and Ocean Sciences, 273.*

Department of Fisheries and Oceans, 2016. Chart No. 1: Symbols, abbreviations, and terms. *Canadian Hydrographic Service, Government of Canada.*

DigitalGlobe, 2016. Accuracy of Worldview Products. *From DigitalGlobe White Papers:* www.digitalglobe.com/resources/white-papers

Grodecki, J., and Dial, G., 2003. Block adjustment of high-resolution satellite images described by rational polynomials. *ASPRS Journal of Photogrammetry and Remote Sensing, 1(10)*, 59-68.

Hedley, J.D., Harborne, A.R., and Mumby, P.J., 2005. Technical note: Simple and robust removal of sun glint for mapping shallow-water benthos. *International Journal of Remote Sensing, 26(10)*, 2107-2112.

Hobi, M.L., and Ginzler, C., 2012. Accuracy assessment of digital surface models based on WorldView-2 and ADS80 stereo remote sensing data. *Sensors, 12*, 6347-6368.

Hodul, M., Bird, S., Knudby, A., and Chénier, R., 2018. Satellite Derived Photogrammetric Bathymetry. *ISPRS Journal of Remote Sensing and Photogrammetry, Under Review*

IHO 2008. Standards for Hydrographic Surveys, *International Hydrographic Organization, Special Publication 44.*

Jacobsen, K., 2017. Problems and limitations of satellite image orientation for determination of height models. *The International Archives of the Photogrammetry, Remote Sensing and Spatial Information Sciences, XLII-1/W1*, 257-264.

Jawak, S.D., and Luis, A.J., 2015. Spectral information analysis for the semiautomatic derivation of shallow lake bathymetry using high-resolution multispectral imagery: A case study of Antarctic coastal oasis. *Aquatic Procedia, 4*, 1331-1338

Jégat, V., Pe'eri, S., Freire, R., Klemm, A., and Nyberg, J., 2016. Satellite-derived bathymetry: Performance and production. *Canadian Hydrographic Conference, May 16-19, Halifax.*

Laporte, J., Hedley, J., and Mouscardès, P., 2015. Satellite derived bathymetry migration: From laboratories to chart production routine. *Hydro International.*

Mavraeidopoulos, A.K., Pallikaris, A., and Oikonomou, E., 2017. Satellite derived bathymetry (SDB) and safety of navigation. *The International Hydrographic Review, 17*, 7-19.

Murase, T., Tanaka, M., Tani, T., Miyashita, Y., Ohkawa, N., Ishiguro, S., Suzuki, Y., Kayanne, H., and Yamano, H., 2008. A photogrammetric correction procedure for light refraction effects at a two-medium boundary. *Photogrammetric Engineering and Remote Sensing, 74(9)*, 1129-1136.

Pacheo, A., Horta, J., Loureiro, J., and Ferreira, Ó., 2015. Retrieval of nearshore bathymetry from Landsat 8 images: A tool for coastal monitoring in shallow waters. *Remote Sensing of Environment, 159*, 102-116.

Pairaud, I., Lyard, F., Auclair, F., Letellier, T., and Marsaleix, P., 2008. Dynamics of the semi-diurnal and quarter-diurnal internal tides in the Bay of Biscay. Part 1: Barotropic tides. *Continental Shelf Research, 28*, 1294-1315.

Pizzolato, L., Howell, S.E.L., Dawson, J., Laliberté, F., and Copland, L., 2016. The influence of declining sea ice on shipping activity in the Canadian Arctic. *Geophysical Research Letters, 43(23)*, 12146-12158.

Polcyn, F.C., Brown, W.L., and Sattinger, I.J., 1970. The measurement of water depth by remote sensing techniques. *Infrared and Optics Laboratory.*

Potuckova, M., 2004. Image matching and its applications in photogrammetry. *Aalborg: Institut for Samfundsudvikling og Planlægning, Aalborg Universitet.*

Said, N.M., Mahmud, M.R., and Hasan, R.C., 2017. Satellite-derived bathymetry: Accuracy assessment on depths derivation algorithm for shallow water area. *The international archives of the Photogrammetry, Remote Sensing, and Spatial Information Sciences, 42*, 159-164.

Stumpf, R.P., Holderied, K., and Sinclair, M., 2003. Determination of water depth with high-resolution satellite imagery over variable bottom types. *Limnology and Oceanography, 47(1)*, 547-556.

Su, H., Liu, H., Wang, L., Filippi, A.M., Heyman, W.D., and Beck, R.A., 2014. Geographically adaptive inversion model for improvising bathymetric retrieval from satellite multispectral imagery. *IEEE Transactions on Geoscience and Remote Sensing, 52(1)*, 465-476.

UKHO, 2015. Satellite Derived Bathymetry. *11th CSPWG Meeting, CSPCWG10-08.7A.*

Vinayaraj, P., Raghavan, V., and Masumoto, S., 2016. Satellite-derived bathymetry using adaptive geographically weighted regression model. *Marine Geodesy, 39(6)*, 458-478.

3.9 Author Contributions

Matus Hodul conducted the research for, and wrote this paper. René Chénier was the manager of the Remote Sensing department at the Canadian Hydrographic Service where much of this work was done, and where funding came from; he provided guidance for the discussion about applications to navigational charting. Marc-André Faucher, Ryan Ahola, Anders Knudby, and Stephen Bird contributed advice and knowledge, as well as assistance with editing.

Chapter 4

Conclusion

An increase in shipping traffic in the Canadian Arctic has led to the need for development of advanced SDB methods to help map nearshore bathymetry in these remote waters. Currently established SDB methods are beginning to be used by hydrographic offices, including the CHS, however these methods carry some limitations which reduce their effectiveness in the Arctic. The empirical method, which creates a regression between depth and a spectral band ratio, requires a great deal of *in-situ* data to calibrate model, and is difficult to implement in areas with heterogeneous sea floor. Physics-based methods, which model light interaction with the water column and sea floor, do not use *in-situ* depth data, but require an extremely precise atmospheric correction, which is often difficult over water, especially at high latitudes.

The aim of this thesis was to develop and test an alternative SDB method which would fill the gap left by the limitations of the two established SDB methods. The proposed method would need to be applicable in areas with highly heterogeneous seafloors, would need to function without precise atmospheric correction, and would need to reach accuracies attainable by the other methods without using *in-situ* data. Satellite photogrammetry is a well established method for mapping terrestrial topography which fulfills these criteria, and this thesis presented a method to extend such a technique underwater for use in SDB.

Chapter 2 provided a detailed description of the proposed photogrammetric bathymetry method, and tested it under ideal conditions in Coral Harbour, Nunavut using WorldView-2 stereo imagery. A four step process was developed, where a standard photogrammetric elevation extraction procedure was followed by a determination of waterline elevation to convert elevation to apparent depth in submerged areas, and a refraction correction to convert the underestimated apparent depth to actual depth. A tidal reduction was then performed to convert from water depths present during image acquisition to bathymetry relative to the local chart datum. In Coral Harbour, this process led to a vertical accuracy of 1.18 m RMSE, with a bias of 3.1 cm. It was found that, though extracted point density reduced with depth as the photogrammetric triangulation algorithm had increasing trouble with feature matching, the vertical accuracy of these points at large depths was not significantly reduced. Additionally, it was found that a single refraction correction factor applied to the entire scene was sufficient for the narrow field-of-view WorldView-2 sensor, yielding only about 1 cm of error at scene edges per 1 m of depth.

Chapter 2 proved the method could work under ideal circumstances, but in order for a remote sensing method to be broadly useful, it must be demonstrated to be robust across many study areas under varying conditions. Chapter 3, *Photogrammetric Bathymetry for the Canadian Arctic*, showed the results of a multi-site analysis of the method's performance, with tests in a different section of Coral Harbour, as well as

Cambridge Bay, Queen Maud Gulf, Arviat, and Frobisher Bay. Except for Frobisher Bay, results in all study areas showed a vertical accuracy of between 0.78 m and 1.16 m RMSE. Wave glint in the Frobisher Bay scene prevented good feature matching during photogrammetric triangulation, so bathymetry mapping failed in that study site. Chapter 3 revealed that the bottom type plays a large role in how successful bathymetric mapping will be, specifically the presence or absence of small, contrasting features in the benthic environment. Feature matching fails in areas with a sandy, smooth seafloor, resulting in gaps in the bathymetry. Fortunately, the empirical method excels in such environments, suggesting that the two methods may be used in conjunction to produce a complete bathymetry map.

This thesis demonstrated that the photogrammetric SDB method is able to achieve vertical accuracies of about 1 m in a variety of locations throughout the Canadian Arctic. These results indicate that the method has a similar or slightly better accuracy than the empirical SDB method currently being used by most hydrographic offices for nearshore charting, while not requiring the *in-situ* data which limits that method to such a degree. The photogrammetric method has also been shown to work well in extremely heterogeneous seafloor environments, where the empirical method largely fails; though in areas of smooth, featureless seafloor where the empirical method excels, the photogrammetric method fails. Thus, for charting applications, it is likely that these two methods will be used in conjunction to produce complete nearshore bathymetry, each being implemented over their respective seafloor type.

Future research into photogrammetric SDB may investigate identifying high-confidence depth point data derived photogrammetrically, and using these to train empirical methods or as part of the modelling in physics-based methods. Further research might also be conducted to test the method using agile satellites other than WorldView, as well as develop a more comprehensive refraction correction, with pixel-specific correction factors to account for variations in geometry across stereo scenes for satellites with a wide field-of-view.